

The effect of droplet configurations within the Functional Renormalization Group of low-dimensional Ising models

Ivan Balog^a and Lucija Nora Farkaš^b

Institute of Physics, P.O.Box 304, Bijenička cesta 46, HR-10001 Zagreb, Croatia

Maroje Marohnić^c

Independent researcher, Zagreb, Croatia

Gilles Tarjus^d

LPTMC, CNRS-UMR 7600, Sorbonne Université, 4 Place Jussieu, 75252 Paris cedex 05, France

(Dated: July 1, 2025)

We explore the application of the nonperturbative functional renormalization group (NPFRG) within its most common approximation scheme based on truncations of the derivative expansion to the Z_2 -symmetric scalar φ^4 theory as the lower critical dimension d_{lc} is approached. We aim to assess whether the NPFRG—a broad, nonspecialized method which is accurate in $d \geq 2$ —can capture the effect of the localized (droplet) excitations that drive the disappearance of the phase transition in d_{lc} and control the critical behavior as $d \rightarrow d_{lc}$. We extend a prior analysis to the next (second) order of the derivative expansion, which turns out to be much more involved. Through extensive numerical and analytical work we provide evidence that the convergence to d_{lc} is nonuniform in the field dependence and is characterized by the emergence of a boundary layer near the minima of the fixed-point effective potential. This is the mathematical mechanism through which the NPFRG within the truncated derivative expansion reproduces nontrivial features predicted by the droplet theory of Bruce and Wallace^{1,2}, namely, the existence of two distinct small parameters as $d \rightarrow d_{lc}$ that control different aspects of the critical behavior and that are nonperturbatively related.

PACS numbers: 11.10.Hi, 75.40.Cx

I. INTRODUCTION

We wish to understand how the nonperturbative functional renormalization group (NPFRG), which is a powerful and versatile approach to study the emergence of scale invariance in a variety of complex systems,^{3,4} fares at describing situations in which the long-distance physics is controlled by highly nonuniform field configurations and localized excitations. We focus on one of the simplest yet physically relevant examples, the approach to the lower critical dimension in the Z_2 -symmetric scalar φ^4 theory which is in the same universality class as the Ising model.

The lower critical dimension of the Ising model is exactly known to be $d_{lc} = 1$ from the Peierls argument.⁵ The one-dimensional physics at low temperature is dominated by the proliferation of localized, instantonic, excitations in the form of kinks and anti-kinks which provide the mechanism for destroying the finite-temperature phase transition. The approach to the lower critical dimension has also been described in detail by Bruce and Wallace^{1,2} through a “droplet” theory, based on the observation that the low-dimensional behavior of the model is controlled by coarse-grained configurations that include droplets of one phase or the other on all scales. At criticality these droplets proliferate and have a nonzero density, their distribution being ruled by the (renormalized) surface tension. Close enough to the lower critical dimension $d_{lc} = 1$, the distribution of droplets can be considered in the dilute limit, which allows Bruce and

Wallace to derive the full droplet distribution. (More precisely, what is then dilute is the droplet boundaries that become in exactly $d_{lc} = 1$ the kinks and anti-kinks corresponding to the one-dimensional instantons.)

A key outcome of the droplet theory is that the critical physics in low dimensions is controlled by two distinct characteristics of the droplets, the fractal dimension of the droplet surface and the critical droplet concentration, which both go to zero as one approaches the lower critical dimension $d_{lc} = 1$ but are nonperturbatively related. Denoting by $\epsilon = d - 1$ the distance from the lower critical dimension, the former is simply given by ϵ while the latter goes as $\exp(-2/\epsilon)/\epsilon$. The presence of two small parameters, exponentially (or equivalently logarithmically) related, is therefore a hallmark of the approach to the lower critical dimension of Ising-like models.

The question that we are interested in is whether the long-distance physics resulting from droplets, kinks and anti-kinks can be captured by the NPFRG which is a theoretical tool based on generic approximation schemes such as the so-called “derivative expansion”. The latter focuses on uniform coarse-grained configurations and slowly varying spatial fluctuations around them that are described through an expansion in gradients of the field.

There have been previous attempts to study the Ising model or the Z_2 -symmetric scalar φ^4 theory in $d = 1$ through the NPFRG and the truncated derivative expansion, but they have only found partial success. Interest in the problem comes from the fact that it also describes the quantum barrier tunneling of a particle in a dou-

ble well potential. The counterpart of the absence of finite-temperature transition is that a particle can never be localized in one minimum for an infinite time even if the barrier height is arbitrarily large. Several works^{6,7} have investigated whether the NPF RG could capture the dependence on the barrier height V of the energy gap between the first excited state and the ground state, a dependence that is known to go as $\exp(-1/V)$. However, whereas good agreement with exact results has been found for small barrier heights,⁶ the predictions worsen as the barrier height increases, even when improving the approximation.^{8–10} Arguments have been given that the truncated derivative expansion in the NPF RG actually cannot reproduce the asymptotic low-temperature scaling associated with the proliferation of kinks and antikinks.¹¹ Also in $d = 1$, attempts to optimize the infrared regulator present in the NPF RG formalism have been unable to recover the (exact) absence of symmetry breaking.¹² A similar problem appears in the NPF RG treatment of a resistively shunted Josephson junction for which one does not correctly capture all regimes of the Schmidt transition.¹³

The issue with the above one-dimensional studies is that nothing guarantees in the NPF RG approach involving approximations such as a truncated derivative expansion that the lower critical dimension is indeed equal to 1. In models where the symmetry that is broken at the transition is continuous as in $O(N > 2)$ field theories, the lower critical dimension $d_{lc} = 2$ and the appearance of Goldstone modes are easily captured by the approximations of the NPF RG. In contrast, the value of d_{lc} when the broken symmetry is discrete depends on the details of the approximation scheme.

In a previous work we have studied the approach to the lower critical dimension and the value of d_{lc} in the Z_2 -symmetric scalar φ^4 theory within the lowest relevant truncation of the derivative expansion which is known as LPA'.¹⁴ At odds with an earlier NPF RG study,¹⁵ we have shown that the convergence of the fixed-point effective action when the dimension $d \rightarrow d_{lc}$ is nonuniform in its field dependence. (Note that this property can only be found because the RG in use is *functional*.) It is characterized by the emergence of a boundary layer around the minima of the fixed-point effective potential whose width goes to zero and whose location moves out to infinity. By means of a singular perturbation analysis we have characterized this behavior and derived an explicit analytical expression for the lower critical dimension d_{lc} whose value depends on the chosen IR regulator and can be fine-tuned to be 1 by tweaking the latter. An important outcome of the boundary-layer mechanism is that the approach to d_{lc} is not described by a unique small parameter but instead involves two logarithmically related vanishing scales, much as predicted by the droplet theory of Bruce and Wallace.

In the present work we extend this analysis of the LPA' approximation to the second order of the derivative expansion. This is of course a necessary step to assess the

robustness and generality of our results. The study, however, turns out to be considerably more difficult. We have gathered strong numerical evidence for the emergence of a boundary layer much like in the LPA' approximation but the singular perturbation treatment is much more involved and we could not manage full numerical and analytical control. As will be presented in detail below, we have nonetheless combined analytical arguments and numerical data to convincingly support the existence of a boundary-layer solution for the fixed-point functions and characterize its properties. Some of the unsatisfactory features of the LPA' appear corrected at the second-order truncation and the critical behavior obtained as $d \rightarrow d_{lc}$ captures several key results of the droplet theory, except for the already mentioned fact that d_{lc} is not generically equal to the exact value of 1. This confirms that at least some of the long-distance physics controlled by strongly nonuniform coarse-grained configurations, involving here droplets on all scales, can be captured within the NPF RG by approximation schemes that at a first glance appear mostly blind to these configurations.

The outline of the paper is as follows. In Section II we give a summary of the NPF RG formalism applied to the approach toward the lower critical dimension of the Z_2 -symmetric scalar φ^4 theory and we introduce the second-order of the derivative expansions, denoted by ∂^2 . In Sec. III we present the singular perturbation treatment of the coupled fixed-point equations for the two functions of the field present at the ∂^2 order and we give numerical evidence for a nonuniform convergence that is characterized by the emergence of a boundary layer around the minima of the effective potential as $d \rightarrow d_{lc}$. We next analyze in detail in Sec. IV the solution of the equations in the boundary layer. In Sec. V we consider the difficult problem of finding the solution in the region where the field is of $O(1)$ and of matching it with the solution in the boundary layer. Based on the solution in the LPA' approximation and some further analytical results we put forward a scenario that appears corroborated by numerical data and we give an estimate of d_{lc} for several choices of infrared regulator. The stability of the fixed point and the behavior of the eigenvalues when $d \rightarrow d_{lc}$ is considered in Sec. VI. Most of the discussion focuses on whether the inverse of the correlation length exponent $1/\nu$ goes to zero as $d \rightarrow d_{lc}$. This is indeed a key property of the exact solution and a prerequisite for observing “essential scaling” in the lower critical dimension. Finally in Sec. VII we summarize the results and give some concluding remarks. The main text is complemented by several appendices where we provide additional detail.

II. FUNCTIONAL RG APPROACH

The Ising universality class is represented in a field-theoretical setting by the Z_2 -symmetric scalar φ^4 action

$$S[\varphi] = \int_x \left[\frac{1}{2} (\partial_\mu \varphi(x))^2 + \frac{r}{2} \varphi(x)^2 + \frac{u}{4!} \varphi(x)^4 \right], \quad (1)$$

where $\int_x \equiv \int d^d x$. We study the critical behavior of this model through the NPMRG^{3,4} which is a modern incarnation of Wilson's renormalization group.¹⁶ In this approach one uses an infrared (IR) regulator function,

$$\Delta S_k[\varphi] = \frac{1}{2} \int_{xy} R_k(x-y) \varphi(x) \varphi(y), \quad (2)$$

with the function R_k obeying several criteria discussed at length in previous works,¹⁷⁻¹⁹ to suppress integration over the fluctuations with momentum less than some running cutoff k in the functional integral defining the partition function of the theory at equilibrium. With the addition of this regulator the partition function now reads

$$Z_k[J] = \int \mathcal{D}\varphi \exp[-S[\varphi] - \Delta S_k[\varphi] + \int_x J(x) \varphi(x)]. \quad (3)$$

The cutoff-dependent effective average action, *i.e.*, the cutoff-dependent generating functional of the 1-particle irreducible (1PI) correlation functions, is given by a modified Legendre transform

$$\Gamma_k[\phi] = -\ln Z_k[J] + \int_x J(x) \phi(x) - \Delta S_k[\phi], \quad (4)$$

with $\phi(x) = \langle \varphi(x) \rangle = \delta \ln Z_k[J] / \delta J(x)$. The flow of the effective average action with the cutoff k obeys an exact FRG equation²⁰⁻²²

$$\partial_t \Gamma_k[\phi] = \frac{1}{2} \int_{xy} \partial_t R_k(x-y) [(\Gamma_k^{(2)}[\phi] + R_k)^{-1}]_{xy}, \quad (5)$$

where $\Gamma_k^{(2)}$ is the second functional derivative of Γ_k and $t = \ln(k/\Lambda)$ with Λ a UV cutoff. At the UV scale, $\Gamma_k[\phi]$ essentially reduces to the bare action whereas when $k = 0$ all the fluctuations have been integrated and one recovers the exact effective action (or Gibbs free-energy functional in the language of magnetic systems).

The exact FRG equation in Eq. (5) is a convenient starting point for nonperturbative approximations.^{18,19,23} A commonly used and generic approximation scheme is based on the truncation of the derivative expansion,

$$\Gamma_k[\phi] = \int_x \left[U_k(\phi(x)) + \frac{1}{2} Z_k(\phi(x)) (\partial_x \phi(x))^2 + \dots \right], \quad (6)$$

where the ellipses denote terms involving a higher number of derivatives of the field. In the present work we focus on the second-order approximation (then dropping all the terms appearing in the ellipses), which we refer to

as ∂^2 for short. Note that this approximation scheme attempts to capture the long-distance physics of the problem by expanding around uniform configurations of the average (also called "classical" or "background") field.

After inserting the ∂^2 ansatz in the exact FRG equation, Eq. (5), one obtains two coupled nonlinear partial differential equations for the functions $U_k(\phi)$ and $Z_k(\phi)$, which are the cutoff-dependent effective potential and field renormalization function respectively. At criticality scale invariance is associated with a fixed point of the FRG flow which can be found by first introducing scaling dimensions and dimensionless quantities,

$$\phi = \frac{k^{(d-2)/2}}{Z_k^{1/2}} \varphi, \quad U_k(\phi) = k^d u_k(\varphi), \quad Z_k(\phi) = Z_k z_k(\varphi), \quad (7)$$

where the flow of Z_k defines the running anomalous dimension,

$$\eta_k = -\frac{\partial_t Z_k}{Z_k}. \quad (8)$$

If a fixed point is indeed found, $\eta_k \rightarrow \eta_*$ when $k \rightarrow 0$, and the scaling dimension of the field is then given by

$$D_\phi = \frac{(d-2+\eta_*)}{2}. \quad (9)$$

(Note that we have used the same notation φ for the bare variable in Eq. (1) and the dimensionless average field, as the former will no longer appear in what follows.)

When expressed in terms of dimensionless quantities, the FRG equations for the effective potential and the field renormalization function take the form

$$\begin{aligned} \partial_t u_k(\varphi) &= -du_k(\varphi) + \frac{(d-2+\eta_k)}{2} \varphi u'_k(\varphi) + \beta_u^{(d)}(\varphi; \eta_k) \\ \partial_t z_k(\varphi) &= \eta_k z_k(\varphi) + \frac{(d-2+\eta_k)}{2} \varphi z'_k(\varphi) + \beta_z^{(d)}(\varphi; \eta_k), \end{aligned} \quad (10)$$

where a prime indicates a derivative with respect to the argument of the function and $\beta_u^{(d)}(\varphi)$ and $\beta_z^{(d)}(\varphi)$ are functions of $w_k(\varphi) = u''_k(\varphi)$, $z_k(\varphi)$, and of their first two derivatives; they are given in Appendix A. The running anomalous dimension η_k is given by the renormalization condition, $z_k(\varphi=0) = 1$, *i.e.*,

$$\eta_k = -\beta_z^{(d)}(\varphi=0; \eta_k). \quad (11)$$

The fixed point is reached when $t = \ln(\frac{k}{\Lambda}) \rightarrow -\infty$ (or $k \rightarrow 0$) and the left-hand sides of the equations in Eqs. (10) go to zero while $\eta_k \rightarrow \eta_*$.

In the present study we have used several forms of regulator with the dimensionless IR cutoff function $r(y = q^2/k^2) = R_k(q^2)/(Z_k q^2)$ chosen as

$$\begin{aligned} r_\Theta(y) &= \alpha \Theta(1-y)(1-y)/y \\ r_e(y) &= \alpha e^{-y}/y \\ r_W(y) &= \alpha \frac{1}{e^y - 1}, \end{aligned} \quad (12)$$

where Θ is the Heaviside step function and α is a variational parameter of order 1. We refer to the above choices as “Theta” or “Litim”,¹⁷ “Exponential”¹⁸, and “Wetterich”²¹ cutoff functions.

For a given value of the dimension d and a chosen IR cutoff function, we can then numerically solve the fixed-point equations and obtain $u_*(\varphi)$, $z_*(\varphi)$, and η_* . For simplicity, we will drop the asterisk to characterize fixed-point quantities in most of the following.

Here we are interested in the approach to the lower critical dimension d_{lc} within the ∂^2 approximation. We have already studied in a previous work¹⁴ a lower order of the derivative expansion, the LPA', in which one describes the effective action through the effective potential $U_k(\phi)$ and a scale-dependent but field-independent field renormalization function Z_k defined through the renormalization condition that $Z_k = Z_k(\phi_{\min,k})$ with $\phi_{\min,k}$ the location of the minimum of the effective potential. (Note that due to the Z_2 symmetry one can restrict the analysis to the positive fields, the situation for negative fields being obtained by symmetry.)

Finally, we comment on a minor point concerning our terminology. When considering exact RG flow equations as Eq. (5) we speak of exact RG (ERG) or functional RG (FRG). After having introduced nonperturbative approximations in the exact FRG, and provided we still deal with functions of the field, we rather use nonperturbative FRG (NPF RG). By construction the exact ERG or FRG is potentially nonperturbative and it would be redundant to then add the qualifier “nonperturbative”.

III. NONUNIFORM CONVERGENCE TO THE LOWER CRITICAL DIMENSION

A. Fixed-point equations as d approaches d_{lc}

When discussing the fixed point of the FRG flow for d approaching the lower critical dimension d_{lc} , it is convenient to introduce the small parameter $\tilde{\epsilon}$,

$$\tilde{\epsilon}(d) = \frac{d - 2 + \eta(d)}{2(2 - \eta(d))} = \frac{D_\phi}{d - 2D_\phi}, \quad (13)$$

where the second equality follows from Eq. (9). One of the hallmarks of a lower critical dimension is that the field does not rescale, *i.e.*, $D_\phi = 0$. Its fluctuations always remain of order 1 in the thermodynamic limit, which prevents ordering. The approach to the lower critical dimension is then described by $\tilde{\epsilon} \rightarrow 0$.

As one expects the relation between d and $\tilde{\epsilon}$ to be monotonic, one can substitute $\tilde{\epsilon}$ for d as a control parameter, which is what we do in our analytic investigations. The starting point of the latter is therefore the set of two coupled differential equations for $u(\varphi)$ and $z(\varphi)$, or more conveniently for the square mass function $w(\varphi) = u''(\varphi)$

and $z(\varphi)$,

$$\begin{aligned} 0 &= -w(\varphi) + \tilde{\epsilon}\varphi w'(\varphi) + \left(\frac{1 + 2\tilde{\epsilon}}{d(\tilde{\epsilon})}\right)\beta_w^{(d(\tilde{\epsilon}))}(\varphi; \eta(\tilde{\epsilon})) \\ 0 &= \eta(\tilde{\epsilon})\left(\frac{1 + 2\tilde{\epsilon}}{d(\tilde{\epsilon})}\right)z(\varphi) + \tilde{\epsilon}\varphi z'(\varphi) + \left(\frac{1 + 2\tilde{\epsilon}}{d(\tilde{\epsilon})}\right)\beta_z^{(d(\tilde{\epsilon}))}(\varphi; \eta(\tilde{\epsilon})) \end{aligned} \quad (14)$$

where $\beta_w^{(d)}(\varphi) = \partial_\varphi^2 \beta_u^{(d)}(\varphi)$, $d(\tilde{\epsilon}) = (1 + 2\tilde{\epsilon})(2 - \eta(\tilde{\epsilon}))$. These two equations are complemented by an equation for the minimum of the effective potential φ_{\min} obtained from $u'(\varphi_{\min}) = 0$ as

$$0 = \tilde{\epsilon}\varphi_{\min} w(\varphi_{\min}) + \left(\frac{1 + 2\tilde{\epsilon}}{d(\tilde{\epsilon})}\right)\partial_\varphi \beta_u^{(d(\tilde{\epsilon}))}(\varphi; \eta(\tilde{\epsilon}))|_{\varphi=\varphi_{\min}} \quad (15)$$

and the renormalization prescription for η : $z(\varphi = 0) = 1$.

When $\tilde{\epsilon} \rightarrow 0$, $d \rightarrow d_{lc}$ and $\eta \rightarrow 2 - d_{lc}$, with d_{lc} now being a quantity to be determined which, due to the approximation, may differ from the exact value $d_{lc} = 1$. One can see that the second term of the ordinary differential equations in Eqs. (14) *a priori* vanishes when $\tilde{\epsilon} \rightarrow 0$. However, one must be careful because the limit may not be uniform in the field φ .

This is precisely what we found in our study of the lower-order approximation LPA'.¹⁴ We observed that the approach to the lower critical dimension involves a boundary layer in the effective potential $u(\varphi)$ around the minima, $\pm\varphi_{\min}$. (Actually, the layers are not quite at the boundary and should rather be called “interior layers”, but we keep the terminology “boundary layers” which is more common.) Such problems can be handled through the singular perturbation theory,^{24,25} which we discuss below.

B. Singular perturbation theory and matching procedure

In the singular perturbation theory of ordinary differential equations, when a control parameter goes to zero,^{24,25} one splits the range of the variable, here the field φ from 0 to ∞ (from now on we restrict ourselves to the positive fields, the negative range being obtained through the Z_2 symmetry), into several regions. In each one of these, a partial solution to the appropriate simplified differential equation when $\tilde{\epsilon} \rightarrow 0$ is looked for. In the present case we expect three distinct regions, large fields $\varphi \gg \varphi_{\min} \rightarrow +\infty$, fields of $O(1)$ with $\varphi < \varphi_{\min}$, and a vanishingly narrow boundary (interior) layer near the minimum φ_{\min} . In the former region, the solution of Eqs. (14) is exactly known at leading order because one simply neglects the beta functions so that one obtains power-law behavior for both w and z , $w(\varphi) \sim \varphi^{1/\tilde{\epsilon}}$ and $z(\varphi) \sim \varphi^{-\eta/\tilde{\epsilon}}$.

In the region including $\varphi = O(1)$ we can neglect the second term in the fixed-point equations and look for a

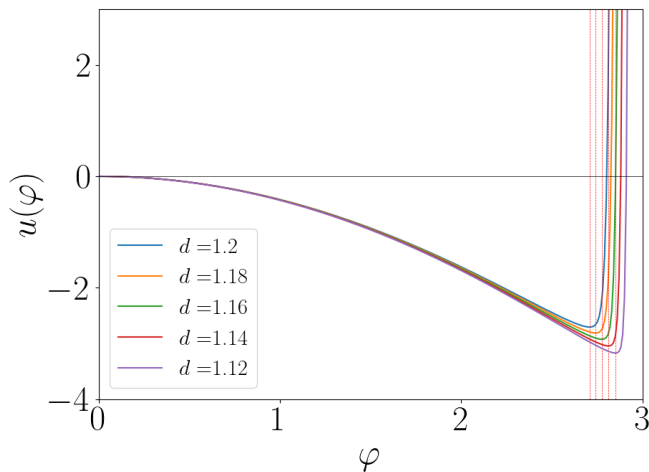


FIG. 1. Numerical result for the fixed-point effective potential $u(\varphi)$ at the ∂^2 order of the derivative expansion when approaching the lower critical dimension. This is illustrated for the Exponential regulator with the prefactor $\alpha = 1$. The vertical dashed lines denote the loci of the minimum of the effective potential for the dimensions shown. The function being symmetric under inversion, we only display positive values of the field.

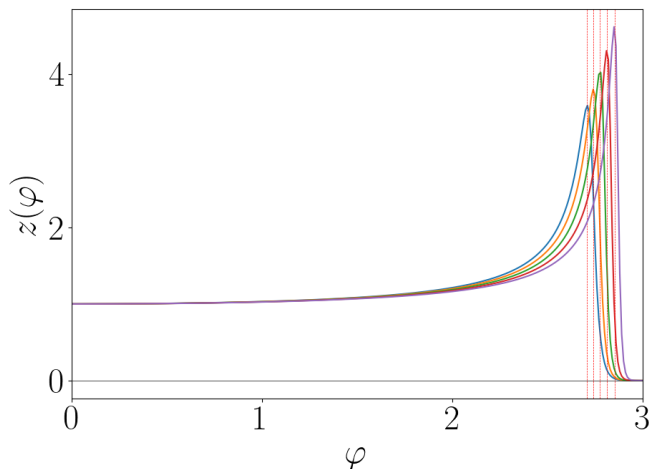


FIG. 2. Numerical result for the fixed-point for the field renormalization function $z(\varphi)$ at the ∂^2 order of the derivative expansion when approaching the lower critical dimension. This is illustrated for the Exponential regulator with the prefactor $\alpha = 1$. The vertical dashed lines denote the loci of the minimum of the effective potential for the dimensions shown. The function being symmetric under inversion, we only display positive values of the field. The color code is the same as in Fig. 1.

solution of the set

$$\begin{aligned} 0 &= -dw(\varphi) + \beta_w^{(d)}(\varphi; \eta) \\ 0 &= \eta z(\varphi) + \beta_z^{(d)}(\varphi; \eta), \end{aligned} \quad (16)$$

where $\eta = 2 - d = -\beta_z^{(d)}(\varphi = 0; 2 - d)$ and d is equal to the (*a priori* unknown) lower critical dimension (all of

this corresponding to $\tilde{\epsilon} = 0$). What makes the present problem more involved than usual singular perturbation theory cases is that not all necessary initial conditions of the differential equations in $\varphi = 0$ are known. The functions being Z_2 symmetric, $w'(0) = 0$ and $z'(0) = 0$, and, as already mentioned, at the ∂^2 order of the derivative expansion we can choose $z(0) = 1$. However, $w(0) = w_0$ is not known; it may still depend on $\tilde{\epsilon}$, which makes the limit $\tilde{\epsilon} \rightarrow 0$ even more complicated, and it must be determined by some matching procedure with the solution in the other regions.

The third region is the narrow layer around the minimum, $|\varphi - \varphi_{\min}| \ll \varphi_{\min}$. In the layer one defines a rescaled variable

$$x = \frac{\varphi - \varphi_{\min}}{\delta(\tilde{\epsilon})}, \quad (17)$$

where $\delta(\tilde{\epsilon}) \rightarrow 0$ is the width of the layer, and this leads to another set of equations at leading order.

All the unknowns should then be fixed by matching the partial solutions in chosen intervals of φ where the regions overlap.^{24,25} As will be detailed below, this is a subtle issue in the present problem at the ∂^2 level.

In the LPA' approximation we could analytically determine the most important features of the fixed-point solution.¹⁴ The solution for the effective potential was obtained at leading order in the three regions discussed above. In the boundary layer near the minimum it is described by

$$u(\varphi) = \delta(\tilde{\epsilon})v(x) \quad (18)$$

with x defined in Eq. (17) and $\delta(\epsilon) = \tilde{\epsilon}\varphi_{\min}$. (Similarly, $w(\varphi) = u''(\varphi) = g(x)/\delta(\epsilon)$ with $g(x) = v''(x)$.) Through a matching procedure between the partial solutions, we found that the location of the minimum diverges in a very slow manner as

$$\varphi_{\min} \sim \sqrt{\ln\left(\frac{1}{\tilde{\epsilon}}\right)} \quad (19)$$

while the boundary-layer width shrinks as $\delta(\tilde{\epsilon}) \sim \tilde{\epsilon}\sqrt{\ln\left(\frac{1}{\tilde{\epsilon}}\right)}$ when $\tilde{\epsilon} \rightarrow 0$. At the same time, the initial value of the square mass function, $w_0 = w(\varphi = 0)$, approaches the pole of the propagator: see below for more detail.

C. Numerical evidence for a boundary-layer scenario at ∂^2 order

We wish to check whether the same scenario as at the LPA' applies at the ∂^2 order. To this end we have numerically determined the fixed-point functions for several IR regulators and solved the set of ordinary nonlinear differential equations for $u(\varphi)$ and $z(\varphi)$ down to the lowest dimensions approaching the (unknown) lower critical dimension for which numerically reliable solutions can be obtained. (This corresponds to small but nonzero values

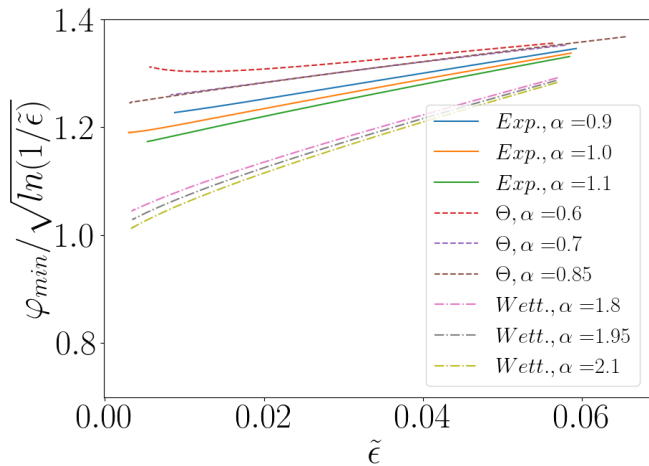


FIG. 3. Dependence on $\tilde{\epsilon}$ of the locus of the minimum of the effective potential, φ_{\min} rescaled by the expected dependence $\sqrt{\ln(1/\tilde{\epsilon})}$ for several choices of regulators at the ∂^2 order of the derivative expansion. All the curves seem to go to nonzero values when $\tilde{\epsilon} \rightarrow 0$.

of $\tilde{\epsilon}$.) The results is illustrated in Fig. 1 for $u(\varphi)$ and in Fig. 2 for $z(\varphi)$. The development of a shrinking layer around the minimum of the potential is clearly visible in both functions.

We have next investigated the characteristics of this emerging layer. We plot in Fig. 3 the minimum of the potential according to the same scaling with $\tilde{\epsilon}$ as in the LPA': see Eq. (19). The figure convincingly shows that the dependence $\varphi_{\min} \sim \sqrt{\ln(1/\tilde{\epsilon})}$ is indeed observed. Another property resulting from the boundary-layer form is that the second and higher-order derivatives of the effective potential evaluated at the minimum diverge with increasing powers of $\delta(\tilde{\epsilon})$ as

$$u^{(p)}(\varphi_{\min}) \propto \frac{1}{\delta(\tilde{\epsilon})^{p-1}}. \quad (20)$$

The outcome is displayed in Fig. 4 for the second and third derivatives of the potential and indeed supports the boundary-layer form with the same dependence on $\tilde{\epsilon}$ as at the LPA' approximation.

We now turn to the boundary layer in the field renormalization function. The emergence of a boundary layer is clearly seen from Fig. 2, with the location of maximum in $z(\varphi)$ being very close to that of the minimum in $u(\varphi)$. The maximum in $z(\varphi)$ grows when $\tilde{\epsilon}$ decreases, but it appears to do so more slowly than $w(\varphi_{\min}) = u''(\varphi_{\min})$. Indeed, we display the ratio $z(\varphi_{\max})/u''(\varphi_{\min})$ in Fig. 5, and the data points to a ratio going to zero as $\tilde{\epsilon} \rightarrow 0$. We characterize this subdominance of $z(\varphi)$ compared to $u''(\varphi) \equiv w(\varphi)$ near the minimum by the factor $\kappa(\tilde{\epsilon})$, *i.e.*, $z(\varphi \approx \varphi_{\min}) \sim \kappa(\tilde{\epsilon})w(\varphi_{\min})$, and we empirically find that this factor goes to zero as $\tilde{\epsilon} \rightarrow 0$ rather slowly, an appropriate

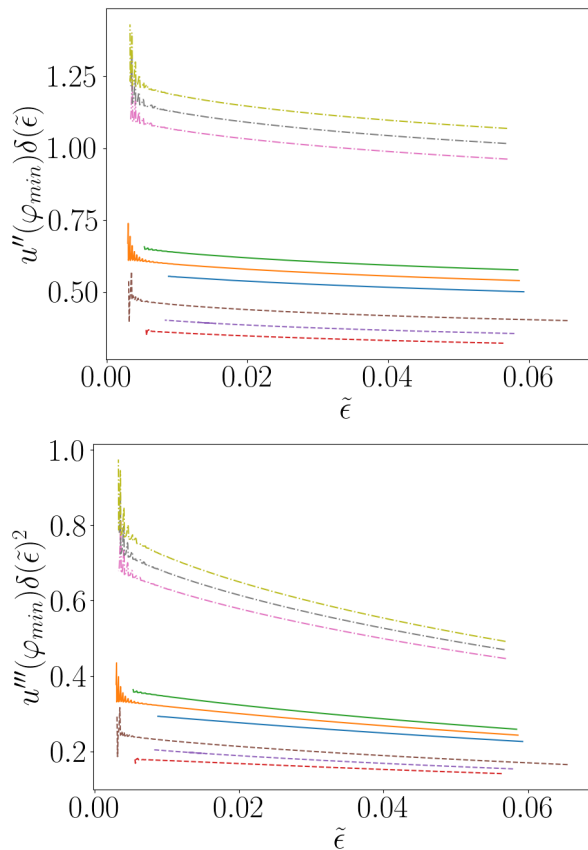


FIG. 4. Dependence on $\tilde{\epsilon}$ of the second (top) and third (bottom) derivatives of the effective potential at the minimum for several choices of regulators (with the same code as in the legend in Fig. 3) at the ∂^2 order of the derivative expansion: $u''(\varphi_{\min})$ is multiplied by the expected boundary-layer width, $\delta(\tilde{\epsilon}) \sim \tilde{\epsilon}\sqrt{\ln(1/\tilde{\epsilon})}$, and $u'''(\varphi_{\min})$ multiplied by the square of the expected boundary-layer width [compare with Eq. (20)]. All the curves seem to go to nonzero values when $\tilde{\epsilon} \rightarrow 0$.

functional form being

$$\kappa(\tilde{\epsilon}) \propto \frac{1}{[\ln(1/\tilde{\epsilon})]^\mu}, \quad (21)$$

with $\mu \approx 2.5$ giving the best data collapse: see Fig. 5.

IV. BOUNDARY LAYER SOLUTION AT ∂^2 ORDER

Based on the above numerical results and on our previous work,¹⁴ we look for a boundary-layer solution near the minimum of the potential in the form

$$w(\varphi) \equiv u''(\varphi) = \frac{g(x)}{\delta(\tilde{\epsilon})} \quad (22)$$

with x given in Eq. (17) and

$$z(\varphi) = \frac{\kappa(\tilde{\epsilon})}{\delta(\tilde{\epsilon})}\zeta(x), \quad (23)$$

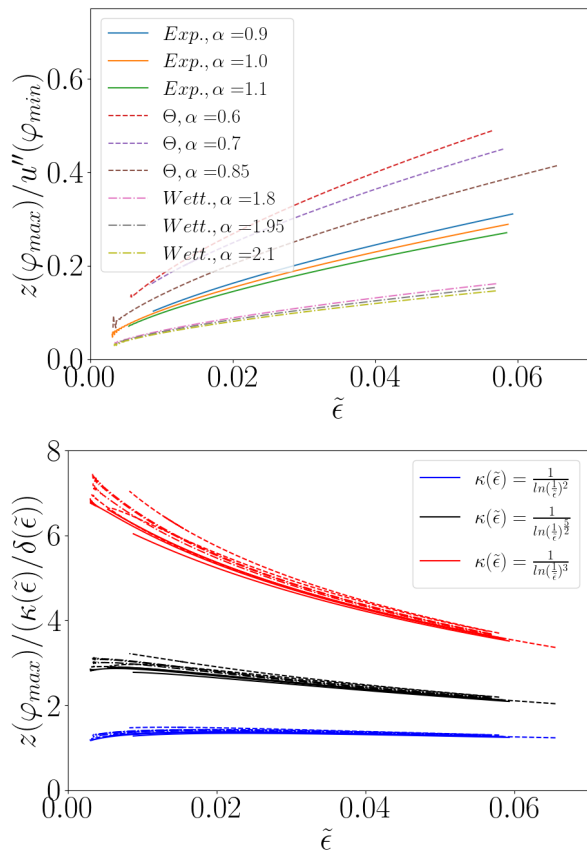


FIG. 5. Evidence showing that the maximum of the field renormalization function $z_{\max} = z(\varphi_{\max})$ grows subdominantly compared to $u''(\varphi_{\min})$ when $\tilde{\epsilon} \rightarrow 0$ for several regulator choices (with the same code as in the legend in Fig. 3). Top: Ratio $z_{\max}/u''(\varphi_{\min})$ versus $\tilde{\epsilon}$; a likely extrapolation is that the ratio goes to zero as $\tilde{\epsilon} \rightarrow 0$. Bottom: Same data further divided by a factor $\kappa(\tilde{\epsilon}) \rightarrow 0$ and illustrated with the functional form $\kappa(\tilde{\epsilon}) \propto [\ln(\frac{1}{\tilde{\epsilon}})]^{-\mu}$, with $\mu = 2, 2.5, 3$; $\mu \approx 2.5$ appears to best collapse the data.

where, by balancing the first two terms of the fixed-point equations for w and z , we can choose $\delta(\tilde{\epsilon}) = \tilde{\epsilon}\varphi_{\min}(\tilde{\epsilon})$ and where $\varphi_{\min}(\tilde{\epsilon}) \rightarrow \infty$ and $\kappa(\tilde{\epsilon}) \rightarrow 0$ in some yet to be determined way as $\tilde{\epsilon} \rightarrow 0$. Note that $\kappa(\tilde{\epsilon})$ is defined up to a multiplicative constant and we can then choose $\zeta(0) = 1$.

The ansatz in Eq. (23) is compatible with the numerical findings displayed in Fig. 5, and we give additional arguments in Appendix B. There, we study two alternative possibilities: 1) $\kappa(\tilde{\epsilon})/\delta(\tilde{\epsilon}) = O(1)$, so that $z = O(1)$ in the boundary layer; 2) $\kappa(\tilde{\epsilon}) = O(1)$, so that z and w scale in the same way. For these two cases we find that there is no possible matching with a physically reasonable solution in the interior interval where $\varphi = O(1)$.

With the above expressions for $w(\varphi)$ and $z(\varphi)$ we can derive the fixed-point equations in the boundary layer in terms of the variable x . Indeed, the dimensionless propagator that appears in the beta functions (see Ap-

pendix A) reads

$$p(y; \varphi) = \frac{1}{y[r(y) + z(\varphi)] + w(\varphi)} \sim \frac{\delta(\tilde{\epsilon})}{g(x) + \kappa(\tilde{\epsilon})\zeta(x)y + \delta(\tilde{\epsilon})yr(y)} \quad (24)$$

where as before y is the dimensionless square momentum. As $\delta(\tilde{\epsilon}) \rightarrow 0$ and $\kappa(\tilde{\epsilon}) \rightarrow 0$ when $\tilde{\epsilon} \rightarrow 0$, we can then simplify the beta functions in the boundary layer. After first rescaling the field φ by a factor $\sqrt{d/(2v_d\alpha A_d)}$, where A_d is a regulator-dependent constant, $A_d = d \int_0^\infty dy y^{d/2} [r(y)/\alpha]$, we obtain the following fixed-point equations at leading order in $\kappa(\tilde{\epsilon})$, $\delta(\tilde{\epsilon})$, and $\tilde{\epsilon}$ (note that we anticipate that $\kappa(\tilde{\epsilon}) \gg \delta(\tilde{\epsilon}) \gg \tilde{\epsilon}$),

$$\begin{aligned} 0 &= -g(x) + g'(x) + \partial_x^2 \left(\frac{1}{g(x)} \right) \\ 0 &= \frac{(2-d)}{d} \zeta(x) + \zeta'(x) - \left[\frac{\zeta''(x)}{g(x)^2} + 4 \frac{\zeta'(x)}{g(x)} \partial_x \left(\frac{1}{g(x)} \right) \right. \\ &\quad \left. + 2\zeta(x) \left(\partial_x \left(\frac{1}{g(x)} \right) \right)^2 \right] \end{aligned} \quad (25)$$

where we have used that $\eta = 2 - d + O(\tilde{\epsilon})$. At the leading order considered here, d should be taken equal to d_{lc} . (Note that the equation for $\zeta(x)$ is linear in $\zeta(x)$ so that, as already stated, one can choose $\zeta(0) = 1$, which simply amounts to a redefinition of $\kappa(\tilde{\epsilon})$ by a constant.)

Similarly, the equation for the location of the minimum [see Eq. (15)] can be written as

$$0 = g(0) - \frac{g'(0)}{g(0)^2}. \quad (26)$$

Note that the equations are now independent of the choice of regulator and that the equation for $g(x)$ is independent from $\zeta(x)$ and is the same as that obtained in the LPA' approximation.¹⁴

To solve the boundary-layer equations we introduce an auxiliary function

$$X(x) = \partial_x \left(\frac{1}{g(x)} \right) + g(x), \quad (27)$$

which satisfies $X'(x) = g(x)$ [because of the first equation in (25)] and $X(0) = 0$ [because of Eq. (26)]. One can then express x as a function of X and define

$$\begin{aligned} a(X) &\equiv \frac{1}{g(x)} \\ b(X) &\equiv \frac{\zeta(x)}{g(x)^2}. \end{aligned} \quad (28)$$

In terms of these new functions $a(X)$ and $b(X)$, the equations in (25) can be rewritten as

$$\begin{aligned} a'(X) - Xa(X) &= -1, \\ b''(X) - Xb'(X) - \frac{2+d}{d}b(X) &= 0. \end{aligned} \quad (29)$$

The solution of the first equation is easily obtained as

$$a(X) = e^{\frac{X^2}{2}} \left(a_0 - \int_0^X dX' e^{-\frac{X'^2}{2}} \right). \quad (30)$$

Interestingly, this form allows us to proceed to the matching with the large-field solution when $\varphi \rightarrow \infty$. The latter is simply obtained from the dimensional part of the fixed-point equations, Eq. (14), which leads to $w(\varphi) \sim \varphi^{1/\tilde{\epsilon}} \rightarrow +\infty$ (see above). Choosing a matching region such that $1/\tilde{\epsilon} \gg x \gg 1$, this imposes that $g(x) \sim e^x$ at large x . As a result $X \rightarrow +\infty$ when $x \rightarrow +\infty$ and $a(X \rightarrow +\infty) \rightarrow 0$. This can only be satisfied if the constant a_0 appearing in the above solution is equal to $\int_0^\infty dX' \exp(-X'^2/2) = \sqrt{\pi/2}$, so that

$$a(X) = e^{\frac{X^2}{2}} \int_X^\infty dX' e^{-\frac{X'^2}{2}}. \quad (31)$$

This is the same solution as found in the LPA' approximation.¹⁴ The solution for $g(x)$ is then obtained by combining the above with Eqs. (27) and (28). From the value in $X = x = 0$, one immediately derives that $g(0) = \sqrt{2/\pi}$ and, from Eq. (26), that $g'(0) = (2/\pi)^{3/2}$. The function $g(x)$ is therefore fully determined but to obtain the corresponding $w(\varphi)$ one further needs $\delta(\tilde{\epsilon})$ and therefore $\varphi_{\min}(\tilde{\epsilon})$.

We next investigate the solution for the function $b(X)$. After introducing the parameter

$$q = \frac{d+2}{d}, \quad (32)$$

we can obtain the solution in the form

$$b(X) = H_{-q} \left(\frac{X}{\sqrt{2}} \right) \hat{b} + {}_1F_1 \left(\frac{q}{2}, \frac{1}{2}, \frac{X^2}{2} \right) \tilde{b}, \quad (33)$$

where \hat{b} and \tilde{b} two constants to be determined, H_{-q} is the Hermite function generalized to negative real degrees [note that $a(X)$ in Eq. (31) can also be expressed as $H_{-1}(X/\sqrt{2})$], and ${}_1F_1$ is Kummer's confluent hypergeometric function. We consider the matching with the large field region where $z(\varphi) \sim \varphi^{-(2-d)/(d\tilde{\epsilon})}$ (see above); when $1/\tilde{\epsilon} \gg x \gg 1$, this implies that $\zeta(x)$ goes to zero as $\exp[-(2/d-1)x]$. From the known asymptotic behavior of the Hermite and hypergeometric functions when $X \gg 1$, we then conclude that $\tilde{b} = 0$ while $\hat{b} > 0$ is constrained by the condition $\zeta(0) = 1$. By using $g(0) = \sqrt{2/\pi}$, $H_{-q}(0) = 2^{-q} \sqrt{\pi} / \Gamma((1+q)/2)$, and Eq. (28) in $X = 0$, we obtain that $\hat{b} = 2^{q-1} \sqrt{\pi} \Gamma((1+q)/2)$.

By expressing the derivative with respect to x in two different ways, *i.e.*, by deriving the right-hand side of the second equation in Eq. (28) or by deriving the solution for $b(X)$ and using that $X'(x) = g(x)$, we arrive at

$$\frac{\zeta'(0)}{g(0)\zeta(0)} = 2\sqrt{\frac{2}{\pi}} - \sqrt{2} \frac{\Gamma(\frac{1+q}{2})}{\Gamma(\frac{q}{2})}, \quad (34)$$

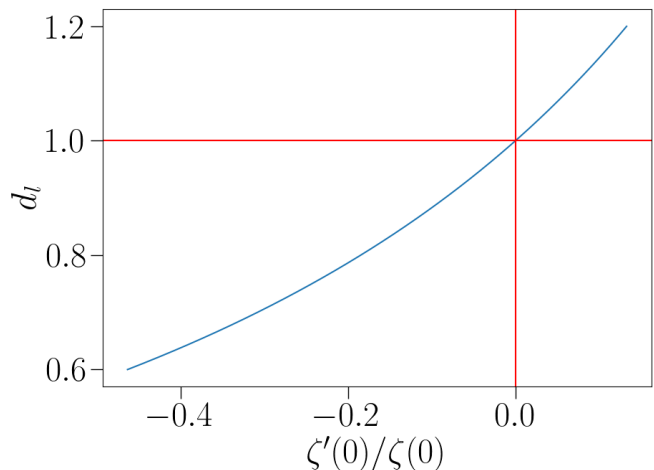


FIG. 6. Relation between the lower critical dimension d_c and the ratio $\zeta'(0)/\zeta(0)$ parametrizing the fixed-point solution for the field renormalization function in the boundary layer, as obtained from Eq. (35).

so that, since $g(0) = \sqrt{\pi/2}$ and $q = (d+2)/d$,

$$\frac{\zeta'(0)}{\zeta(0)} = 2 \left[1 - \frac{\Gamma(\frac{3}{2})\Gamma(1+\frac{1}{d})}{\Gamma(\frac{1}{2}+\frac{1}{d})} \right], \quad (35)$$

where $d \equiv d_c$.

While the solution for $g(x)$ is fully determined by the matching procedure with the large-field region, this is not the case for the function $\zeta(x)$ which is still parametrized by d_{lc} . Equivalently, this means that the value of the lower critical dimension is not simply determined by considering the boundary-layer solution and the matching with the large-field region, as it was in the LPA' approximation.¹⁴ (In the LPA' the renormalization prescription for the field renormalization function, which is otherwise taken as independent of the field, is chosen at the minimum of the potential, $z(\varphi_{\min}) = 1$, and therefore within the boundary layer.)

We plot in Fig. 6 the monotonic relation between d_{lc} and the parameters of the fixed-point solution for the field renormalization function in the boundary layer $\zeta'(0)/\zeta(0)$ given in Eq. (35). Interestingly, the exact value $d_{lc} = 1$ is recovered if the minimum of the potential corresponds to an extremum of z , *i.e.*, $\zeta'(0) = 0$, but there is no *a priori* reason to select this value.

To obtain a full solution over the whole field interval $[0, \infty)$ one needs to solve the equation outside the boundary layer in the region including fields of $O(1)$ and to match this partial solution with the boundary-layer solution in a region where $1 \ll \varphi \ll \varphi_{\min}$ (as we anticipate that φ_{\min} diverges when $\tilde{\epsilon} \rightarrow 0$, see Fig. 3) and $x \rightarrow -\infty$, *e.g.*, $\varphi_{\min} - \varphi = O((\tilde{\epsilon}\varphi_{\min})^a)$ with $0 < a < 1$.

When $x \rightarrow -\infty$, one easily finds that

$$g(x) \sim \frac{1}{\sqrt{2}|x|\sqrt{\ln(|x|)}} \rightarrow 0 \quad (36)$$

and

$$\zeta(x) \sim \frac{[\ln(|x|)]^{\frac{2-d}{2d}}}{|x|} \rightarrow 0, \quad (37)$$

so that in the matching region $w(\varphi) \sim O((\tilde{\epsilon}\varphi_{\min})^{-a})$ is much larger than 1 and $z(\varphi) \sim \kappa(\tilde{\epsilon})O((\tilde{\epsilon}\varphi_{\min})^{1-2a})$ is also very large if $a > 1/2$ and κ is only slowly going to zero.

Matching with the solution of the equation derived for $\varphi=O(1)$ is thus possible only if the latter can reach field values $\varphi \gtrsim \varphi_{\min}$ and if in the matching region both the square mass w and the field renormalization function z are very large when $\tilde{\epsilon} \rightarrow 0$. As we will see, this turns out to be very stringent constraints at the ∂^2 order of the derivative expansion. This is somehow expected because one still needs to determine several quantities: d_{lc} or $\zeta'(0)$, $\delta(\tilde{\epsilon})$ or equivalently $\varphi_{\min}(\tilde{\epsilon})$, $\kappa(\tilde{\epsilon})$, and the initial condition w_0 in $\varphi = 0$.

V. MATCHING PROCEDURE AT ∂^2 ORDER

A. Summary of the procedure in the LPA' approximation

In the LPA' approximation where the field renormalization is a scale-dependent but field-independent parameter fixed by $z(\varphi_{\min}) = 1$, the only two remaining unknowns are $\varphi_{\min}(\tilde{\epsilon})$ and w_0 and they should be fixed (at leading order) by finding a solution of the $\varphi=O(1)$ region that matches the boundary-layer solution when φ approaches φ_{\min} .¹⁴ The equation to be solved is the first one of Eq. (16), which explicitly reads

$$w(\varphi) = \frac{2v_d}{d} \partial_\varphi^2 \ell_0^{(d)}(w(\varphi); \eta = 2 - d), \quad (38)$$

where $\ell_0^{(d)}$ is a threshold function involving the IR regulator and is defined as (see Appendix A)

$$\ell_0^{(d)}(w(\varphi); \eta) = -\frac{1}{2} \int_0^\infty dy y^{\frac{d}{2}} \frac{\eta r(y) + 2yr'(y)}{y[z + r(y)] + w} \quad (39)$$

with $z \equiv 1$; $d = d_{lc}$ is known from the boundary-layer solution which is itself fully determined by the matching with the large-field region where the beta functions vanish: see above and [14].

The function $\ell_0^{(d)}(w; \eta = 2 - d)$ being monotonically decreasing with w , Eq. (38) can be turned into the equation of motion for an anharmonic oscillator, φ playing the role of time, from which one derives the key properties:¹⁴

- All solutions $w(\varphi)$ are periodic with a half period φ_* that depends on the initial condition w_0 .
- The half-period φ_* can become very large and $w_* = w(\varphi_*)$ very large as well, both conditions

being required for matching the boundary-layer solution with $\varphi_{\min} \gg 1$ and $w(\varphi_{\min}) \sim 1/\delta(\tilde{\epsilon}) \gg 1$, provided w_0 approaches closely enough the pole w_P of the propagator $p(y; \varphi) = [y(1 + r(y)) + w]^{-1}$: $w_0 = w_P + \rho(\tilde{\epsilon})$, where $\rho(\tilde{\epsilon} \rightarrow 0) \rightarrow 0^+$ in a manner that depends on the detailed form of the IR cutoff function $r(y)$.

- When φ_* and w_* are both very large, one can show that $\varphi_* \sim \sqrt{\ln w_*}$.

A global solution of the fixed-point equation requires one to match the solution just obtained with that in the boundary layer. As already stressed it however represents an unusual form of singular perturbation theory because the initial value w_0 is not known and moreover still depends on the small parameter $\tilde{\epsilon}$ (in an equation which is otherwise considered at $\tilde{\epsilon} = 0$). The matching needs $\varphi_* \gtrsim \varphi_{\min}$ and $w_* \gtrsim w(\varphi_{\min})$ and the overlap region where the two solutions should coincide at leading order is such that all these quantities are very large (see also above). In this limit it is easily seen that the equations derived with $\varphi = O(1)$ and that in the boundary layer coincide. The equations are the same but the boundary conditions are w_* in φ_* for the former and $w(\varphi_{\min}) = 1/(\tilde{\epsilon}\varphi_{\min})$ in φ_{\min} for the latter. Matching is then automatically guaranteed by taking

$$w_* \sim w(\varphi_{\min}) = 1/(\tilde{\epsilon}\varphi_{\min}) \quad \text{and} \quad \varphi_* \sim \varphi_{\min}. \quad (40)$$

With the property that $\varphi_* \sim \sqrt{\ln w_*}$ this immediately leads to $\varphi_{\min} \sim \sqrt{\ln[1/(\tilde{\epsilon}\varphi_{\min})]}$, hence $\varphi_{\min} \sim \sqrt{\ln(1/\tilde{\epsilon})}$ at dominant order.

We conclude this recap by three remarks. First, this represents a weak form of matching because only orders of magnitude are matched. Going beyond this would be very involved. Second, the periodic solution of the $\tilde{\epsilon} = 0$ equation has itself a boundary layer around the half period φ_* with a width $1/w_*$ that goes to zero as w_0 approaches the pole of the propagator and w_* diverges. In the matching region, the solution of the (physical) boundary layer and that of the boundary layer of the periodic solution coincide, being both given by Eq. (36). Finally, the fact that w_0 approaches the pole of the propagator is expected on physical ground for the lower critical dimension where the critical and the zero-temperature ordered fixed points merge.¹⁴

B. Scenario for matching at ∂^2 order

At the ∂^2 order singular perturbation theory requires us to consider the equations in (15) when dropping the second terms in $\tilde{\epsilon}\varphi\partial_\varphi$ and neglecting terms of order $\tilde{\epsilon}$. As already stressed, w_0 is unknown, but the matching with the boundary layer solution should fix $\delta(\tilde{\epsilon})$ [or equivalently $\varphi_{\min}(\tilde{\epsilon})$], $\kappa(\tilde{\epsilon})$, and d_{lc} [or $\zeta'(0)$]: see above.

We again anticipate that a requirement for a possible matching is that w_0 approaches the pole w_P of the propagator. We find, however, that this is very hard to achieve

while (numerically) getting solutions that are physically acceptable. We have been unable to obtain a rigorous resolution of the problem. Actually, the fine-tuning of the value of d_{lc} that provides a proper matching appears so demanding (with severe numerical instabilities developing when $w_0 \rightarrow w_P$) that our procedures are unable to find a definite answer. (Note that, as a result, we cannot exclude the possibility that the fixed-point equations stop having a solution when $\tilde{\epsilon}$ is at and below a very small but nonzero threshold, *i.e.*, slightly before reaching d_{lc} .)

Lacking strong enough analytical and numerical control of the solutions, we thus make a tentative set of hypotheses based on the numerical findings shown in Sec. III and the scenario found at the LPA' order:

- The relevant solution of the set of equations obtained by dropping the $\tilde{\epsilon}\varphi\partial_\varphi$ terms is periodic with a half period φ_* that depends on the initial condition w_0 . It is denoted by $(\bar{w}(\varphi), \bar{z}(\varphi))$.
- When w_0 approaches the pole w_P of the propagator, the half-period φ_* , as well as $w_* = \bar{w}(\varphi_*)$ and $z_* = \bar{z}(\varphi_*)$ can become very large, with nonetheless $z_* \ll w_*$.
- The existence of a periodic solution when $w_0 \rightarrow w_P$ (and $\tilde{\epsilon} \rightarrow 0$) requires the selection of a unique, and of course regulator-dependent, value d_{lc} .
- Furthermore, when φ_* and w_* are both very large, they are related by $\varphi_* \sim \sqrt{\ln w_*}$.

Before giving evidence supporting the above hypotheses, we explore their consequences. First, one easily realizes that in the matching region between the periodic and the boundary-layer solutions, where $1 \ll \varphi \ll \varphi_*$, φ_{\min} , $1 \ll w \ll w_*$, $w(\varphi_{\min})$, $1 \ll z \ll z_*$, $z(\varphi_{\min})$ with $z \ll w$, the equations are identical because the terms in $\tilde{\epsilon}\varphi\partial_\varphi$ are always negligible. The difference is of course in the boundary values that are taken in φ_* for the periodic solution $(\bar{w}(\varphi), \bar{z}(\varphi))$ and in φ_{\min} for the boundary-layer solution. Matching between the two types of solutions is then automatically achieved if $\varphi_* \sim \varphi_{\min}$, $w_* \sim w(\varphi_{\min})$, and $z_* \sim z(\varphi_{\min})$. With the last assumption that $\varphi_* \sim \sqrt{\ln w_*}$, this immediately yields

$$\varphi_{\min} \sim \sqrt{\ln\left(\frac{1}{\tilde{\epsilon}}\right)} \quad \text{and} \quad \delta(\tilde{\epsilon}) \sim \tilde{\epsilon} \sqrt{\ln\left(\frac{1}{\tilde{\epsilon}}\right)}, \quad (41)$$

as at the LPA' level of approximation and as well confirmed numerically (see Sec. III C). On the other hand, in the absence of more detailed information concerning the actual analytical form of the periodic solution $\bar{z}(\varphi)$, we are unable to determine the scaling of $\kappa(\tilde{\epsilon})$.

C. Searching for periodic solutions of the equations derived for $\varphi = O(1)$

We now discuss evidence supporting the scenario presented above. We have looked for periodic solutions of

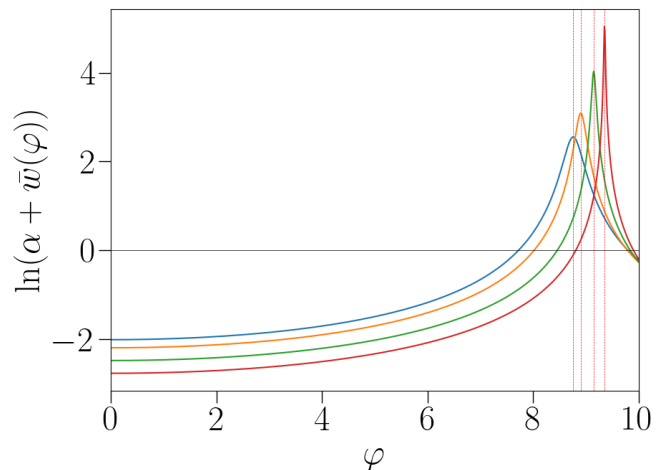


FIG. 7. Periodic solution of Eq. (42): $\ln(\alpha + \bar{w}(\varphi))$ versus φ for $d = 0.8$ and the Litim/Theta regulator with $\alpha = 0.7$. The different curves represent different initial conditions of $w_0 > w_P = -\alpha$. As w_0 approaches closer to the pole of the propagator w_P , the half-period φ_* at which \bar{w} is maximum shifts to higher values while $w_* = \bar{w}(\varphi_*)$ rapidly increases. We only show the periodic function in a range of field between 0 and somewhat above the half-period which is marked by a vertical dashed line.

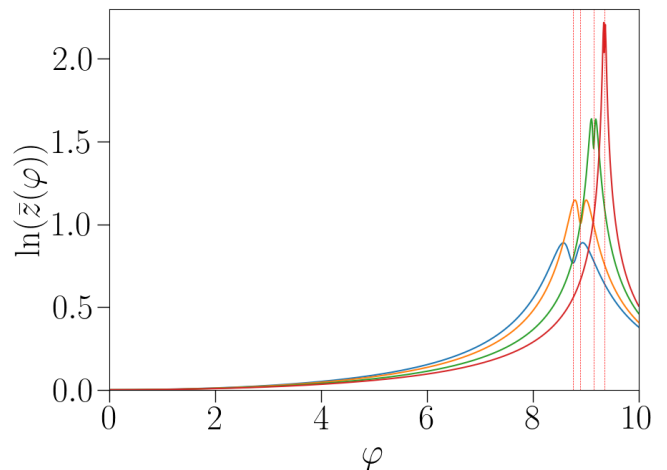


FIG. 8. Periodic solution of Eq. (42): $\ln(\bar{z}(\varphi))$ versus φ for $d = 0.8$ and the Litim/Theta regulator with $\alpha = 0.7$. The curves correspond to the same initial conditions $w_0 > w_P = -\alpha$ as in Fig. 7 and the half-period φ_* is in each case the same as for \bar{w} . Note that \bar{z} has a minimum in φ_* and first passes through a maximum for a value which is very close to φ_* . The value $z_* = \bar{z}(\varphi_*)$ increases as w_0 approaches closer to the pole of the propagator $w_P = -\alpha$. We only show the periodic function in a range of field between 0 and somewhat above the half-period which is marked by a vertical dashed line.

the set of equations when the terms in $\tilde{\epsilon}\varphi\partial_\varphi$ are dropped. This turns out to be an extremely hard numerical task

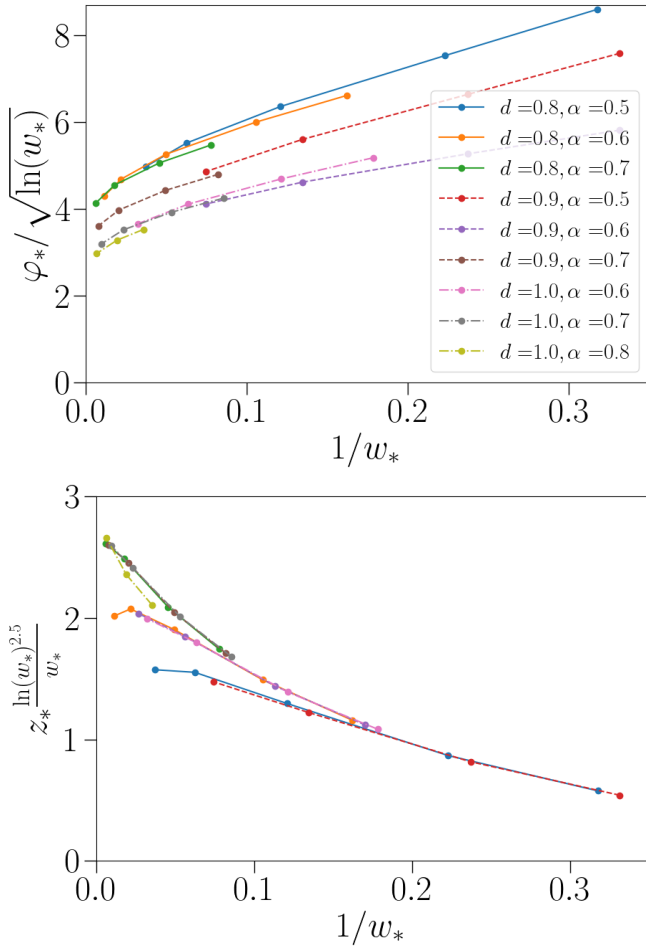


FIG. 9. Properties of the periodic solution of Eq. (42) found for a range of d and of the prefactor α of the Litim/Theta regulator (given in the legend of the top panel). Top: Variation with $1/w_*$ of the half-period φ_* scaled by the anticipated factor $\sqrt{\ln w_*}$, where $w_* = \bar{w}(\varphi_*)$. Bottom: Variation with $1/w_*$ of $z_* = \bar{z}(\varphi_*)$ scaled by the factor $w_*/(\ln w_*)^\mu$ with $\mu \approx 2.5$.

when w_0 approaches the pole w_P of the propagator. We have then lifted the condition that $\eta = 2 - d$ (which corresponds to $\tilde{\epsilon} = 0$) and searched for solutions of the equations

$$\begin{aligned} w(\varphi) &= \frac{2v_d}{d} \partial_\varphi^2 \ell_0^{(d)}(w(\varphi); z(\varphi); \eta), \\ 0 &= \eta z(\varphi) + \beta_z^{(d)}(\varphi; \eta), \end{aligned} \quad (42)$$

where we have explicitly displayed the first equation only, the beta function $\beta_z^{(d)}$ being too long to be worth giving here (see i Appendix A). The equations should be solved with initial conditions $w(0) = w_0$, $w'(0) = 0$, $z(0) = 1$, $z'(0) = 0$, and we fine-tune the value of η to find periodic solutions $\bar{w}(\varphi)$ and $\bar{z}(\varphi)$ with the (same) half period φ_* . We call $\eta_\#(d, w_0)$ the value at which this is achieved. Keeping d fixed we then repeat the procedure for smaller and smaller values of w_0 , thereby approaching as close as

possible the pole w_P and obtaining a sequence of values $\eta_\#(d, w_0)$ and the corresponding periodic solutions.

We have followed this numerical procedure for the Theta/Litim regulator for which rather bulky but analytically explicit equations can be obtained. We have done it for a range of the regulator parameter α . For each choice of α , d , and w_0 , we have then used Wolfram Mathematica to solve the system by adaptive Runge-Kutta methods of high order. We have obtained periodic solutions for a range of dimensions $0.8 \leq d \leq 1.0$ with $0.5 \leq \alpha \leq 0.8$. In Figs. 7 and 8 we illustrate the outcome for $w(\phi)$, $z(\phi)$ with $d = 0.8$, $\alpha = 0.7$, and several values of w_0 (in this case the pole of the propagator is in $y = 0$ and $w_P = -\alpha$). For better clarity we plot $\ln(w(\phi) - w_P)$ and $\ln(z(\phi))$ versus ϕ .

The solutions display the anticipated properties from the scenario put forward above. As w_0 approaches closer to the pole w_P the half-period φ_* at which \bar{w} is maximum shifts to higher values while $w_* = \bar{w}(\varphi_*)$ rapidly increases and so does $z_* = \bar{z}(\varphi_*)$. (Note that $\bar{z}(\varphi)$ has a local minimum at the half-period φ_* , a local maximum being present for a value slightly less than φ_* , and of course slightly more due to the periodic nature of the solution.) An important feature that appears to be confirmed is the last item of the scenario in Sec. VB, *i.e.*, $\varphi_* \sim \sqrt{\ln w_*}$ when $w_* \gg 1$: see Fig. 9 (top). Fig. 9 (bottom) further illustrates that z_* increases more slowly than w_* , in a manner that is actually compatible with what is found in the numerical results for the full solution in the boundary layer (see Fig. 5), $z_* \sim w_*/[\ln w_*]^\mu$ with $\mu \approx 2.5$.

As already alluded to when discussing the LPA' case, the periodic solutions to the set of equations obtained by dropping the terms in $\tilde{\epsilon}\varphi\partial_\varphi$ display an emergent boundary layer around the half-period φ_* when w_0 approaches the pole w_P . The analytic solution of this boundary layer is discussed in Appendix C. As it should (see Sec. VB), this boundary-layer solution and the boundary-layer solution of the full set of fixed-point equations derived in Sec. IV coincide at leading order in the matching region where $1 \ll \varphi \ll \varphi_*$, φ_{\min} , $1 \ll w \ll w_*$, $w(\varphi_{\min})$, and $1 \ll z \ll z_*$, $z(\varphi_{\min})$, provided $\varphi_* \sim \varphi_{\min}$, $w_* \sim w(\varphi_{\min})$, and $z_* \sim z(\varphi_{\min})$.

Several additional comments are worth making. First, the numerical procedure for obtaining periodic solutions seems to be limited by the formation of boundary layers near the extrema of the functions \bar{w} and \bar{z} when the pole w_P is approached (see Appendix C). We have found that the procedures used for solving the equations are limited to 16 digits of accuracy, but higher precision would be needed to resolve the solution accurately when w_* and z_* exceed certain values, which leads to increasingly sharper variations in the φ dependence.

Second, we can further address the motivations to focus on periodic solutions: Why wouldn't another kind of solution be a good candidate for the matching procedure? We have investigated this question along trajectories $\eta(d, w_0)$ which for a chosen d (and of course α) are either above or below the trajectory $\eta_\#(d, w_0)$ associ-

ated with periodic solutions. We have generically found that when w_0 approaches the pole, if η is just slightly above $\eta_{\#}(d, w_0)$, then the solution $z(\varphi)$ diverges at some finite φ , which causes $w(\varphi)$ to diverge as well. If on the other hand η is just slightly below $\eta_{\#}(d, w_0)$, then $z(\varphi)$ becomes negative at some finite φ , which is unphysical. The conclusion is that periodic solutions appear to be the only ones that make physical sense as w_0 approaches the pole w_P . Furthermore, when the value of w_* is large as w_0 approaches the pole, the variation $\delta\eta_{\#}$ around $\eta_{\#}$ that is sufficient to drive the solution in either of the above unphysical regimes becomes extremely small, as illustrated in Fig. 10.

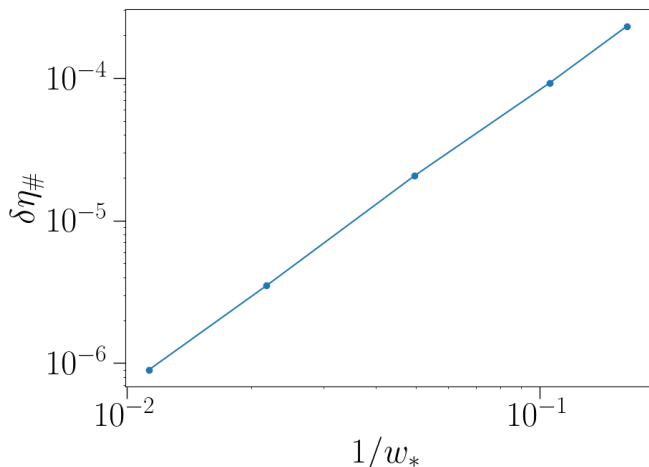


FIG. 10. Estimate of the variation $\delta\eta_{\#}$ around the periodic-solution value $\eta_{\#}$ for which the solution falls into either of the unphysical regimes described in the text when w_* becomes very large (as w_0 approaches the pole of the propagator). Here, $d = 0.8$ and $\alpha = 0.6$. Note that this is a log-log plot.

All of this being said, one still needs to check that (for a given IR regulator) the periodic solution persists up to the end of the trajectory $\eta_{\#}(d, w_0)$ when $\eta_{\#}(d, w_0) = 2 - d$ and $w_0 \rightarrow w_P$. This would correspond to the desired fixed-point solution that can be matched with the boundary-layer one (see above). We display our results in Fig. 11 where we plot $d - 2 + \eta_{\#}$ versus $1/w_*$ for the already discussed periodic solutions that, as we have stressed, we are able to obtain for a limited range of d and of the regulator parameter α only (we use the Litim/Theta regulator). In principle the value of the lower critical dimension $d_{lc}(\alpha)$ is that for which $d - 2 + \eta_{\#} = 0$ when $1/w_* = 0$. One can see that this seems to exclude the value $d = 1$ because $d - 2 + \eta_{\#}$ vanishes for a small yet nonzero $1/w_*$. The other combinations of (d, α) could be viable candidates but this requires extrapolating the data in some form or another. As we have already encountered in this problem, there could be a steep approach to zero with a diverging derivative with respect to $1/w_*$, *e.g.*, where

$(d - 2 + \eta_{\#})$ times w_* goes as $\ln(w_*)$ to some power. For the Litim/Theta regulator considered here the data for $d = 0.8$ and 0.9 is compatible with such a behavior.

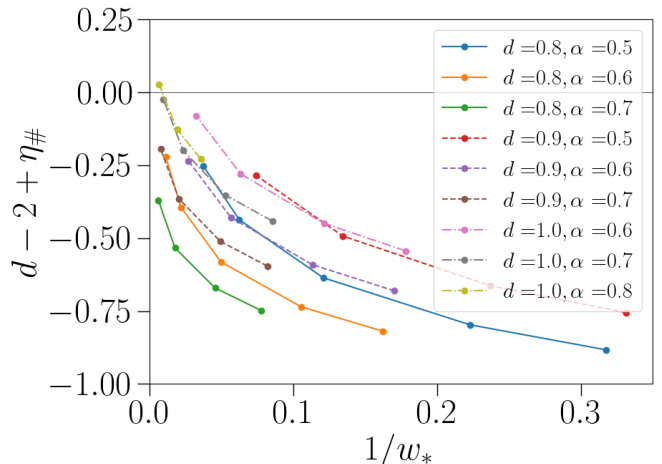


FIG. 11. Variation of $d - 2 + \eta_{\#}$ with $1/w_*$ down to the lowest values of $1/w_*$ for which a periodic solution can be found. An acceptable fixed-point solution at the lower critical dimension should have $d - 2 + \eta_{\#} = 0$ when $1/w_* = 0$. The data are obtained for a range of values of d and of the prefactor α of the Litim/Theta regulator.

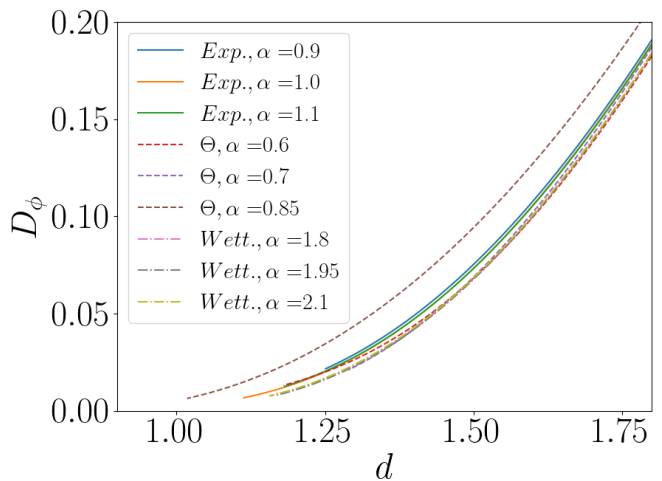


FIG. 12. Scaling dimension of the field D_{ϕ} versus space dimension d from the solution of the fixed-point equations at ∂^2 order for the three IR regulators, Theta/Litim, Exponential, and Wetterich, and a range of prefactor α .

D. More on the estimate of d_{lc} at ∂^2 order

We now go back to the numerical results obtained by numerically solving the full fixed-point equations for d

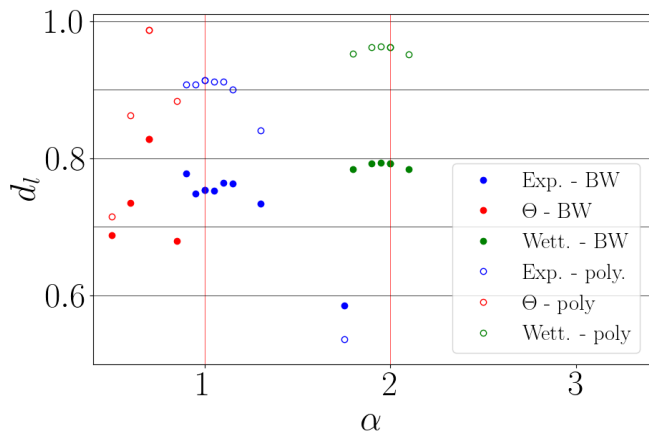


FIG. 13. Estimates of the lower critical dimension d_{lc} from extrapolations of the curves D_ϕ versus d shown in Fig. 12 for the three IR regulators, Theta/Litim (red symbols), Exponential (blue symbols), and Wetterich (green symbols). The open and filled circles correspond to fits using a second-order polynomial and Eq. (43), respectively.

as low as possible. We illustrate the dependence of the field scaling dimension $D_\phi = (d - 2 + \eta)/2 \approx d\tilde{\epsilon}$ on the dimension d in Fig. 12 for the three regulators and a range of prefactors α . From this plot, the lower critical dimension d_{lc} is estimated by extrapolating the curves to the point where $D_\phi = 0$. The most naive way to proceed is to use a (quadratic) polynomial fit to extrapolate the data and this gives a first set of estimates.

Before investigating an alternative formula to extrapolate the data we need to make a detour and discuss the possible connection of our FRG approach with the droplet theory of Bruce and Wallace.^{1,2} As already stressed, a key result of the latter is that the approach to the lower critical dimension is controlled by two small parameters that are nonperturbatively related: the fractal dimension of the droplet surface, which goes as $d - d_{lc}$ and controls the vanishing of the critical temperature T_c and of the inverse of the correlation length exponent $1/\nu$, and the critical droplet concentration which controls the scaling dimension of the field $D_\phi = (d - 2 + \eta)/2$. The two are related by

$$D_\phi \propto \frac{1}{d - d_{lc}} e^{-\frac{2}{d - d_{lc}}}, \quad (43)$$

where in this exact calculation, $d_{lc} = 1$. Inverting the relation yields

$$d - d_{lc} \propto \frac{1}{\ln(\frac{1}{D_\phi})}, \quad (44)$$

which in particular leads to T_c and $1/\nu$ going to zero as $1/\ln(\frac{1}{D_\phi})$ when $D_\phi \rightarrow 0$ and $d \rightarrow 1$.

Interestingly, the solutions of the FRG fixed-point equations at the LPA' and ∂^2 orders also have several

small parameters that are associated with the peculiar boundary-layer form that emerges as one approaches d_{lc} . The natural parameter is $\tilde{\epsilon}$ which, up to a factor of d , is equal to D_ϕ . Another one is $1/\ln(1/\tilde{\epsilon})$ which appears in the characteristics of the boundary layer. As already discussed in the previous work on the LPA' approximation, the critical temperature T_c can be related in the FRG to the field at the minimum of the effective potential, φ_{\min} , as¹⁴

$$T_c \propto \frac{1}{\varphi_{\min}^2}, \quad (45)$$

which predicts that $T_c \propto 1/\ln(\frac{1}{\tilde{\epsilon}}) \propto 1/\ln(\frac{1}{D_\phi})$. This is the same relation as found by the droplet theory.

This correspondence with the droplet theory suggests fitting the data for D_ϕ versus d to the formula in Eq. (43). The outcome for $d_{lc}(\alpha)$ is shown in Fig. 13 together with the result of the fit to a second-order polynomial. The difference between the two procedures is of about 15% and we note that we obtain values that are systematically below the exact result $d_{lc} = 1$.

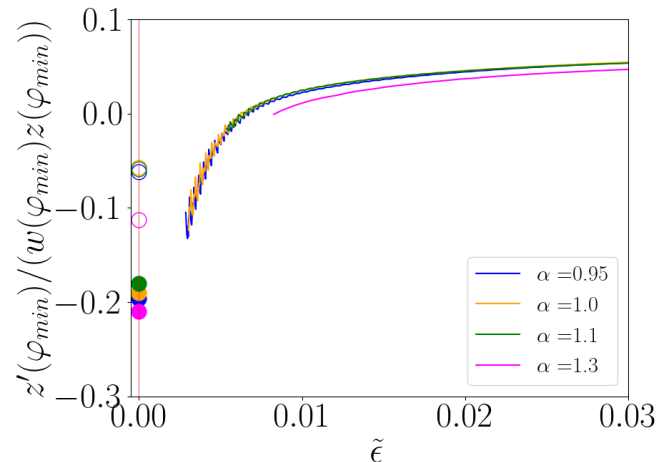


FIG. 14. Ratio $z'(\varphi_{\min})/[w(\varphi_{\min})z(\varphi_{\min})]$ versus $\tilde{\epsilon}$ as obtained for small but nonzero values of $\tilde{\epsilon}$ from the solution of the full fixed-point equations at ∂^2 order with the Exponential regulator and several values of the prefactor α . In $\tilde{\epsilon} = 0$ we display the right-hand side of Eq. (46) with the estimates of $d_{lc}(\alpha)$ found in Fig. 13 either via a polynomial fit (open circles) or via Eq. (43) (filled circles).

To further constrain the estimate of $d_{lc}(\alpha)$ we use the relation that we have derived through the boundary-layer analysis of the fixed-point equations, Eq. (34). Switching back from the boundary-layer functions to the original ones, one can rewrite Eq. (34) as

$$\frac{z'(\varphi_{\min})}{w(\varphi_{\min})z(\varphi_{\min})} = 2\sqrt{\frac{2}{\pi}} - \sqrt{2} \frac{\Gamma(1 + \frac{1}{d_{lc}})}{\Gamma(\frac{1}{2} + \frac{1}{d_{lc}})}. \quad (46)$$

The left-hand side is accessible from the fixed-point solutions at small but nonzero $\tilde{\epsilon}$. Extrapolating its

dependence on the latter down to $\tilde{\epsilon} = 0$ should give d_{lc} via the expression in the right-hand side. We have carried out this calculation for the Exponential regulator and a range of values of α . The data are plotted in Fig. 14 together with the expected values of the right-hand side for d_{lc} obtained above from fitting either a polynomial or Eq. (43). For the lowest $\tilde{\epsilon}$ that could be accessed (for $\alpha = 0.95 - 1.1$) the data clearly seem to exclude the estimates of d_{lc} found with the polynomial fit and are more compatible with the fit through Eq. (43). However, it appears difficult at this point to more tightly constrain the value of $d_{lc}(\alpha)$.

VI. STABILITY ANALYSIS OF THE FIXED POINT

A. Generalities for the ∂^2 approximation

As usual, the stability of the fixed point is investigated by introducing a perturbation, $w_k(\varphi) = w(\varphi) + k^\lambda \delta w(\varphi)$, $z_k(\varphi) = z(\varphi) + k^\lambda \delta z(\varphi)$, $\eta_k = \eta + k^\lambda \delta \eta$, where w , z , and η are the fixed-point quantities, and linearizing the FRG flow equations, Eqs. (10) and (11), with respect to the perturbation. The problem turns into an eigenvalue determination with λ corresponding to a relevant direction if it is < 0 and to an irrelevant one if it is > 0 . For a more compact notation we define $f_1(\varphi) = \delta w(\varphi)$ and $f_2(\varphi) = \delta z(\varphi)$, $y_1 = -(2 - \eta)$ and $y_2 = \eta$ and we then obtain the eigenvalue equations as

$$0 = \delta \eta A_i(\varphi) + (y_i - \lambda) f_i(\varphi) + \frac{d-2+\eta}{2} \varphi f'_i(\varphi) + \sum_{j=1,2} [a_{ij}(\varphi, \eta) + b_{ij}(\varphi, \eta) \partial_\varphi + c_{ij}(\varphi, \eta) \partial_\varphi^2] f_j(\varphi), \quad (47)$$

where $i = 1, 2$, and where the functions $A_i(\varphi)$, $a_{ij}(\varphi, \eta)$, $b_{ij}(\varphi, \eta)$, and $c_{ij}(\varphi, \eta)$ are derived from the beta functions $\beta_w^{(d)}(\varphi; \eta)$ and $\beta_z^{(d)}(\varphi; \eta)$ with the final expressions evaluated at the fixed point; more details are given in Appendix D, but the important property is that the A_i 's, a_{ij} 's, and c_{ij} 's are even in φ while the b_{ij} 's are odd.

The above set of equations can be rewritten in a matrix form as

$$-\delta \eta \mathbf{A}(\varphi) = (\mathbf{y} - \lambda \mathbf{I}) \mathbf{f}(\varphi) + \frac{d-2+\eta}{2} \varphi \mathbf{f}'(\varphi) + [\mathbf{a}(\varphi, \eta) + \mathbf{b}(\varphi, \eta) \partial_\varphi + \mathbf{c}(\varphi, \eta) \partial_\varphi^2] \mathbf{f}(\varphi) \quad (48)$$

where \mathbf{y} is the diagonal matrix with elements y_1 and y_2 and \mathbf{I} is the identity matrix. The matrix \mathbf{c} has for elements $c_{11} = -2v_d \ell_1^{(d)}(\varphi; \eta)$, $c_{12} = 2v_d \partial \ell_0^{(d)}(\varphi; \eta) / \partial z(\varphi)$, $c_{21} = 0$, $c_{22} = -2v_d \ell_1^{(d)}(\varphi; \eta)$, so that its determinant is equal to $[2v_d \ell_1^{(d)}(\varphi; \eta)]^2$ and is strictly positive, which ensures that the matrix is invertible (see Appendix D). One can therefore recast the equa-

tion as

$$\left(\mathbf{I} \partial_\varphi^2 + \mathbf{c}(\varphi, \eta)^{-1} [\mathbf{b}(\varphi, \eta) + \frac{d-2+\eta}{2} \varphi] \partial_\varphi + \mathbf{c}(\varphi, \eta)^{-1} \times [\mathbf{a}(\varphi, \eta) + (\mathbf{y} - \lambda \mathbf{I}) \right] \mathbf{f}(\varphi) = -\delta \eta \mathbf{c}(\varphi, \eta)^{-1} \mathbf{A}(\varphi), \quad (49)$$

which is the canonical form of a linear second-order differential equation with coefficients that are continuous over \mathbb{R} . Due to the symmetry property of the coefficients, the eigenvectors can be sorted out into even and odd under the inversion of φ . Note that one expects a discrete set of eigenvalues. After fixing the initial conditions $\mathbf{f}(0) = \mathbf{f}_0$ and $\mathbf{f}'(0) = \mathbf{f}'_0$, there is a unique solution defined over the whole range of φ but it exists for any $\lambda, \delta \eta \in \mathbb{R}$. The selection of the possible discrete set of eigenvalues and of the associated $\delta \eta$ comes from considering the behavior at large field.²⁶ Generically, the solution for $f_{i=1,2}(\varphi)$ is a linear combination of a power law and a growing exponential [e.g., for f_1 , $\varphi^{(\lambda+d)/(d\tilde{\epsilon})}$ and $\exp(K_d \tilde{\epsilon}^2 \varphi^{2+2/\tilde{\epsilon}})$ with K_d a constant of $\mathcal{O}(1)$]. Requiring that the coefficient of the exponential be zero in both f_1 and f_2 is then expected to restrict the allowed values of λ to a discrete set and fix the associated $\delta \eta$.

Consider first the odd sector. When evaluated in $\varphi = 0$, the left-hand side of Eq. (49) is equal to zero while $\mathbf{c}(\varphi = 0, \eta)^{-1} \mathbf{A}(\varphi = 0) \neq 0$. As a result one must have $\delta \eta = 0$. One relevant eigenvalue is trivially obtained because it is associated with derivatives of the fixed-point functions: $f_1(\varphi) = K w'(\varphi)$ and $f_2(\varphi) = K z'(\varphi)$. It is easy to check by taking a derivative with respect to φ of the fixed point equation that $\lambda = -(d-2+\eta)/2$ which is minus the scaling dimension D_ϕ of the field (in the effective action this is associated with a φ^3 perturbation). This eigenvalue goes to zero at the lower critical dimension when $\tilde{\epsilon} = 0$.

For the even sector, we expect that there is a single relevant eigenvalue which is related to the correlation-length exponent ν by $\lambda = -1/\nu$. A key feature of the approach to the lower critical dimension in the exact theory is that $1/\nu \rightarrow 0$. This is a prerequisite for the so-called ‘‘essential scaling’’ that is observed at the lower critical dimension, $d = d_{lc}$. This scaling means that, the critical temperature T_c being equal to zero, the correlation length ξ still diverges as one approaches zero temperature but in an exponential rather than a power-law fashion,

$$\xi \sim \exp(\Delta/T), \quad (50)$$

where Δ is the energy scale of the localized excitations (kinks and anti-kinks) that proliferate and destroy the finite-temperature transition in $d_{lc} = 1$. In the droplet theory,^{1,2} $1/\nu$ goes to zero as $d-1$ when $d \rightarrow 1$. As explained in Sec. VD, when translated in the small parameter $\tilde{\epsilon} \propto D_\phi$, this implies that $1/\nu \sim 1/\ln(1/\tilde{\epsilon})$ due to the nonperturbative relation between $\tilde{\epsilon}$ and $d - d_{lc}$. At the LPA' level,¹⁴ we showed that $1/\nu = 0$ in $\tilde{\epsilon} = 0$ but the numerical results pointed to an approach in $\delta(\tilde{\epsilon}) \sim \tilde{\epsilon} \sqrt{\ln(1/\tilde{\epsilon})}$ instead of $1/\ln(1/\tilde{\epsilon})$. (In this approximation T_c and $1/\nu$ appear to go to zero with

qualitatively different dependences on $\tilde{\epsilon}$, contrary to the exact result.)

Before discussing the eigenvalue problem within the framework of singular perturbation theory we give the numerical results obtained by solving the eigenvalue equations for fixed d as close as possible to the lower critical dimension.

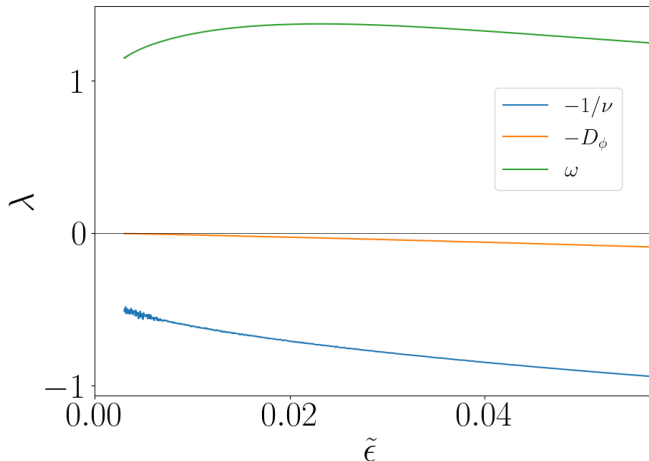


FIG. 15. Variation with $\tilde{\epsilon}$ of the first three eigenvalues around the critical fixed point: $\lambda = -D_\phi$ in the odd sector as well as $\lambda = -1/\nu$ and $\lambda = \omega$ in the even sector. We have used the Exponential regulator with prefactor $\alpha = 1$.

B. Numerical results

We have studied the stability of the critical fixed point as one lowers the dimension d . From $d = 4$ down to the lowest possible d for which we can determine the fixed point we find two and only two relevant directions around the critical fixed point: one is in the odd sector, and corresponds to $\lambda = -(d - 2 + \eta)/2 = -D_\phi$, and one is in the even sector, and can be associated with $-1/\nu$. All of the other eigenvalues are strictly positive, *i.e.*, irrelevant; they stay of order 1 and do not appear to go to zero as d approaches d_{lc} . We plot for illustration in Fig. 15 the three first eigenvalues, $-D_\phi$, $-1/\nu$, and the leading correction to scaling ω , for the Exponential regulator with $\alpha = 1$ in the vicinity of d_{lc} ($\tilde{\epsilon} \lesssim 0.5$). The correction-to-scaling exponent ω is close to 1 and rather constant over the interval of $\tilde{\epsilon}$. The eigenvalue $-D_\phi$ goes to zero as $-d\tilde{\epsilon}$ when $\tilde{\epsilon} \rightarrow 0$. On the other hand, the behavior of $-1/\nu$ is more ambiguous. It decays when $\tilde{\epsilon}$ decreases but it still of the order of -0.5 at the lowest accessible values of $\tilde{\epsilon}$. The extrapolation to zero in $\tilde{\epsilon} = 0$ is therefore nontrivial, if it is indeed true that $1/\nu = 0$ in this limit within the ∂^2 approximation. This will be addressed in more detail in the next subsection.

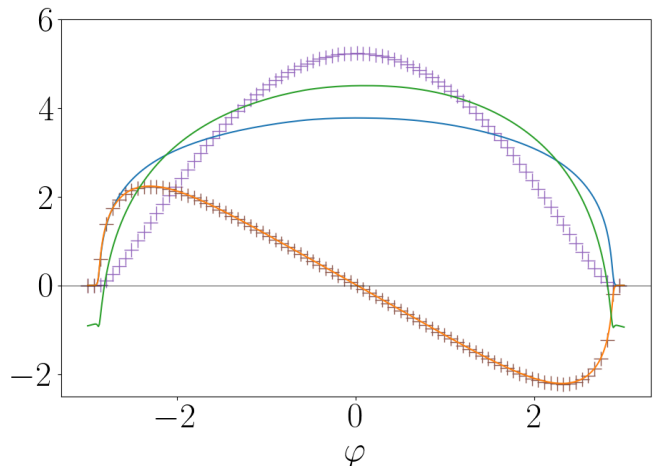


FIG. 16. Eigenvectors associated with the first three eigenvalues in the direction of the function $w(\varphi)$ for $d = 1.113$ where $\tilde{\epsilon} = 0.00301$: For improved clarity we plot $\delta w(\varphi)/[\alpha + w(\varphi)]^2$ for $\lambda = -D_\phi$ (dark red symbols), $\lambda = -1/\nu$ (purple symbols) and $\lambda = \omega$ (full green line). For comparison we also plot the even function $1/[\alpha + w(\varphi)]$ (full blue line) and the odd one $w'(\varphi)/[\alpha + w(\varphi)]^2$ (full orange line, which is virtually indistinguishable from the eigenvector associated with $\lambda = -D_\phi$). We have used the Exponential regulator with prefactor $\alpha = 1.0$.

We next look at the shape of the three eigenvectors associated with the eigenvalues $-D_\phi$, $-1/\nu$, and ω . In Fig. 16 we display the eigenvectors in the direction of the perturbation of the function w , *i.e.*, $\delta w(\varphi)$, for a very small value of $\tilde{\epsilon} \approx 0.003$. For a better visualization we actually plot $\delta w(\varphi)/(\alpha + w(\varphi))^2$ and we use both positive and negative φ to make the symmetry of the functions clearer. We first note that all the eigenvectors appear to show a change of behavior near $|\varphi| \approx 2.9$, which corresponds to the location the minimum of the effective potential for this value of $\tilde{\epsilon}$. This is likely stemming from the emergence of the boundary layer already discussed at length. Next, the two eigenvectors associated with the relevant eigenvalues appear to go to zero when $|\varphi|$ is large, contrary to the eigenvector associated with the irrelevant eigenvalue ω which goes to a value of $O(1)$. Remembering that the large-field behavior of the fixed-point function $w(\varphi)$ goes as $|\varphi|^{1/\tilde{\epsilon}}$ while that of the eigenvector $\delta w(\varphi)$ goes as $|\varphi|^{(1+\lambda/d)/\tilde{\epsilon}}$ (see above), this corresponds to the expected behavior for the relevant eigenvalues with $\lambda < 0$ while for the correction-to-scaling eigenvalue it implies that $\omega \approx d$ [since $\delta w(\varphi)/(\alpha + w(\varphi))^2 \sim |\varphi|^{(-1+\lambda/d)/\tilde{\epsilon}}$].

As anticipated, the odd eigenvector associated with the eigenvalue $\lambda = -D_\phi$ is proportional to the first derivative of the fixed-point function $w(\varphi)$: the two curves shown in Fig. 16 are indistinguishable. A potentially more interesting observation which we will refine below is that the even eigenvector associated with $\lambda = -1/\nu$ appears very similar to the odd one when φ is near the minima of the effective potential, *i.e.*, in the boundary layer regions.

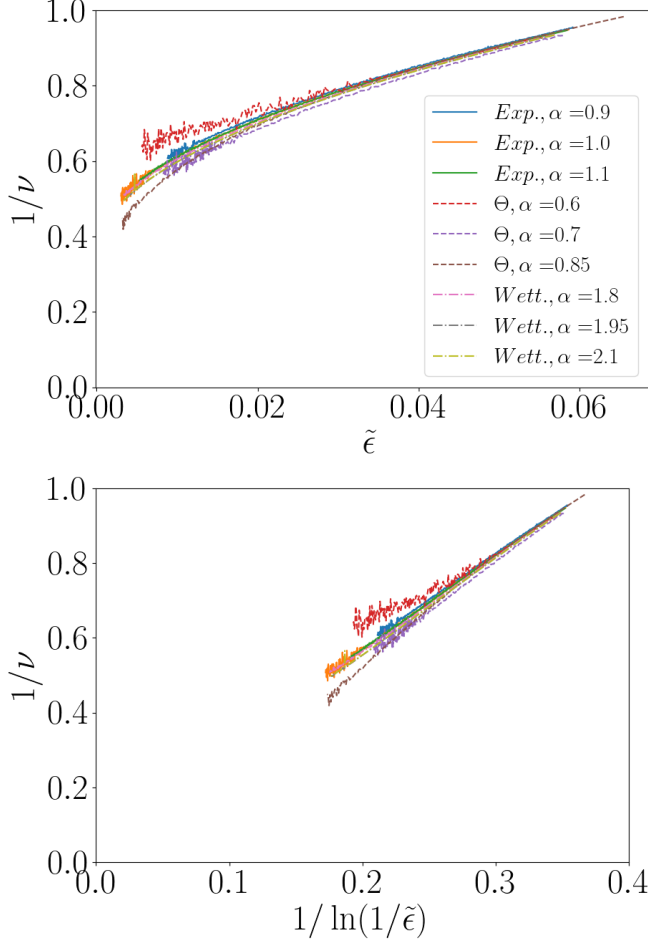


FIG. 17. Variation of $1/\nu$ as one approaches the lower critical dimension for several regulator choices in the ∂^2 approximation. Top: $1/\nu$ versus $\tilde{\epsilon}$. Bottom: Same data plotted as $1/\nu$ versus $1/\ln(1/\tilde{\epsilon})$.

C. Does $1/\nu \rightarrow 0$ when $\tilde{\epsilon} \rightarrow 0$ at ∂^2 order?

The main issue concerning the stability of the critical fixed point is whether $1/\nu \rightarrow 0$ as $d \rightarrow d_{lc}$ and $\tilde{\epsilon} \rightarrow 0$. As already stressed this is the exact behavior with $d_{lc} = 1$ and it is a prerequisite for observing an essential scaling at the lower critical dimension.

In Fig. 17 we display data for $1/\nu$ that is obtained for several regulators and for values of $\tilde{\epsilon}$ as small as possible. We plot the data in two different ways. In the top figure we show $1/\nu$ versus ϵ . As already noticed when discussing Fig. 15, it is hard to decide whether $1/\nu$ can go to zero when extrapolating to $\tilde{\epsilon} = 0$; all curves do appear to bend down when $\tilde{\epsilon}$ decreases but the values of $1/\nu$ reached for the lowest accessible $\tilde{\epsilon}$ are still of order 0.4-0.6. A fit to a dependence in $\delta(\tilde{\epsilon}) \sim \tilde{\epsilon}\sqrt{\ln(1/\tilde{\epsilon})}$ (as numerically found satisfactory at the LPA' level) clearly gives a strictly positive value of $1/\nu$ in $\tilde{\epsilon} = 0$.

In the bottom figure we next plot $1/\nu$ versus $1/\ln(1/\tilde{\epsilon})$.

This is motivated by the droplet theory^{1,2} which predicts that

$$\frac{1}{\nu} \sim \left[\frac{1}{\ln(1/\tilde{\epsilon})} \right]. \quad (51)$$

As seen from the figure, such a behavior is more compatible with our data, and plausible linear extrapolations to $\tilde{\epsilon} = 0$ indeed give intercepts close to $1/\nu = 0$. This is suggestive but by no means conclusive. We thus take an additional angle on the problem by studying in more detail the eigenvalue equations and the eigenvectors associated with the relevant perturbations.

D. Singular perturbation analysis

As done before for the fixed-point equations, we now turn to a singular perturbation analysis of the eigenvalue equations when $\tilde{\epsilon} \rightarrow 0^+$. We again expect that the eigenvectors associated with the two relevant eigenvalues can be separately studied in three domains –fields of $O(1)$, large fields, and boundary layer around the minimum φ_{\min} of the effective potential– with a full solution then obtained by matching the partial ones in the regions where they overlap.

Consider the boundary layer around the minimum. We expect that the eigenvectors can be written as the fixed-point functions in the form

$$\begin{aligned} \delta w(\varphi) &= \frac{\delta g(x)}{\delta(\tilde{\epsilon})} \\ \delta z(\varphi) &= \frac{\kappa(\tilde{\epsilon})}{\delta(\tilde{\epsilon})} \delta \zeta(x) \end{aligned} \quad (52)$$

with $x = (\varphi - \varphi_{\min})/\delta(\tilde{\epsilon})$. Inserting this in the eigenvalue equations and using the same scaling analysis as for the fixed-point functions, we find at leading order

$$\begin{aligned} 0 = & - \left(1 + \frac{\lambda}{d}\right) \delta g(x) + \delta g'(x) + \delta \left[\partial_x^2 \left(\frac{1}{g(x)} \right) \right] \\ & + C_d \frac{\delta \eta}{\tilde{\epsilon}} g'_*(x) + O(\kappa(\tilde{\epsilon}), \delta \eta) \end{aligned} \quad (53)$$

and

$$\begin{aligned} 0 = & \left(\frac{2-d}{d} + \frac{\lambda}{d} \right) \delta \zeta(x) + \delta \zeta'(x) - \delta \left[\frac{\zeta''(x)}{g(x)^2} + 4 \frac{\zeta'(x)}{g(x)} \times \right. \\ & \left. \partial_x \left(\frac{1}{g(x)} \right) + 2\zeta(x) \left(\partial_x \left(\frac{1}{g(x)} \right) \right)^2 \right] + C_d \frac{\delta \eta}{\tilde{\epsilon}} \zeta'_*(x) \\ & + O(\kappa(\tilde{\epsilon}), \delta \eta) \end{aligned} \quad (54)$$

where $\delta[\dots]$ denotes the linear variation due to the perturbations around the fixed-point functions, *e.g.*, $\delta \left[\partial_x^2 (1/g(x)) \right] = -\partial_x^2 (\delta g(x)/g_*(x)^2)$, and we have momentarily reinstalled the notation g_* , ζ_* and w_* , z_* for the fixed point.

Note that contrary to what happens in the LPA' approximation,¹⁴ $\delta\eta$ is not determined by the behavior in the boundary layer only, as we have chosen the conventional renormalization prescription at ∂^2 order that the running anomalous dimension is fixed by the condition in $\varphi = 0$, $z_k(\varphi = 0) = 1$ implying $\delta z(\varphi = 0) = 0$.

As shown above, for the odd eigenvector associated with $\lambda = -D_\phi \approx -d\tilde{\epsilon}$, one rigorously finds that $\delta\eta = 0$. In this case, a solution of Eqs. (53,54) is provided by $\delta g(x) = Kg'_*(x)$, $\delta\zeta(x) = K\zeta'_*(x)$, with the eigenvalue $\lambda = 0$ at the leading order. More generally, any solution of this kind with $\lambda = 0$ is valid provided $\delta\eta/\tilde{\epsilon} \rightarrow 0$ when $\tilde{\epsilon} \rightarrow 0$. A possible scenario, which is borne out in the LPA' approximation (see below), is then that to the same partial solution in the boundary layer correspond two distinct global solutions, one odd and one even; the partial solutions differ in the region where $\varphi = O(1)$ while nonetheless matching with similar boundary-layer solutions in the relevant domain of overlap.

Unfortunately, at the ∂^2 level we cannot go much further with the singular perturbation treatment. Indeed, as discussed in detail in Sec. V, we already do not have full analytical and numerical control of the fixed-point solutions themselves. Assuming that $\delta\eta/\tilde{\epsilon} \rightarrow 0$ and $\lambda \rightarrow 0$ when $\tilde{\epsilon} \rightarrow 0$, it seems plausible that the set of second-order linear equations obtained from Eq. (49) for fields of $O(1)$,

$$\left(\mathbf{I} \partial_\varphi^2 + \mathbf{c}(\varphi, \eta)^{-1} \mathbf{b}(\varphi, \eta) \partial_\varphi + \mathbf{c}(\varphi, \eta)^{-1} [\mathbf{a}(\varphi, \eta) + \mathbf{y}] \right) \mathbf{f}(\varphi) = 0, \quad (55)$$

with initial condition $\delta z(0) = 0$, has one even solution on top of the odd one (recall that we are looking for solutions able to match with the boundary-layer ones, which themselves should match with the power-law solutions at large field).

If no definite conclusion comes from this treatment at the ∂^2 level, it is worth showing how this works at the LPA' level, where we can get an analytic solution.

E. A detour by the singular perturbation treatment at the LPA' level

Here we build on our previous work in [14] and provide new results as well.

At the LPA', one only needs the equation for $w_k(\varphi)$ and η_k . We look for odd and even eigenperturbations with an eigenvalue equal to zero when $\tilde{\epsilon} = 0$. As mentioned above this can be achieved in the boundary layer by choosing $\delta w(\varphi) = Kw'(\varphi)$ or in a scaled form $\delta g(x) = Kg'(x)$ (where $w(\varphi)$ and $g(x)$ denote the fixed-point functions). This solution matches at large field with the relevant power-law behavior $\delta w(\varphi) \sim \varphi^{1/\tilde{\epsilon} + O(1)}$ when $\lambda = 0$ and $\tilde{\epsilon} \rightarrow 0^+$. This is possible because one can also show that within the boundary layer $\delta\eta = 0$ at leading order: see Appendix E.

The odd or even property of the eigenvector under Z_2 field inversion is determined by the solution around $\varphi = 0$ and for fields of $O(1)$. The eigenvalue equation at leading order when $\tilde{\epsilon} = 0$ (with $\lambda = 0$) reads

$$0 = -d\delta w(\varphi) - 2v_d \frac{\partial^2}{\partial \varphi^2} [\ell_1^{(d)}(\overline{w}(\varphi)) \delta w(\varphi)], \quad (56)$$

with $\ell_1^{(d)}(w) = -\partial_w \ell_0^{(d)}(w)$, while the corresponding fixed-point equation satisfied by $\overline{w}(\varphi)$ is

$$0 = -d\overline{w}(\varphi) + 2v_d \frac{\partial^2}{\partial \varphi^2} [\ell_0^{(d)}(\overline{w}(\varphi))], \quad (57)$$

where the overline denotes the periodic fixed-point solution for $\varphi = O(1)$ and $\tilde{\epsilon} \rightarrow 0$. An odd eigenvector is obviously given by $\delta w(\varphi) = K\overline{w}'_*(\varphi)$ and it matches with the solution in the boundary layer. It is easy to show that there is also an even eigenvector of the form $\delta w(\varphi) = c(\varphi)\overline{w}_*(\varphi)$ with

$$\begin{aligned} c(\varphi) &\sim \frac{c_0}{\varphi}, \quad \text{if } \varphi \rightarrow 0 \\ &\sim c_1, \quad \text{if } 1 \ll \varphi \ll \varphi_*, \end{aligned} \quad (58)$$

with c_0 and c_1 two constants, and where φ_* is the half-period of the fixed-point solutions (we only consider the range $\varphi \geq 0$ due to the symmetry). More details are given in Appendix E. This solution matches with the boundary-layer one when $1 \ll \varphi \ll \varphi_*$ (provided the fixed-point solution $\overline{w}(\varphi)$ itself matches with the fixed-point solution in the boundary layer, which imposes a condition on $w(\varphi = 0)$ ¹⁴).

The singular perturbation treatment thus provides us with one odd and one even eigenvector associated with the eigenvalue $\lambda = 0$ when $\tilde{\epsilon} \rightarrow 0$, with both eigenvectors being proportional to the first derivative of the fixed-point function in the boundary layer around the minimum of the potential. This is this latter property that we will now check in the case of the ∂^2 level of approximation.

F. Further numerical evidence for $1/\nu = 0$ in $\tilde{\epsilon} = 0$ at ∂^2 order

We now go back to our numerical study of the eigenvectors at small but nonzero $\tilde{\epsilon} = 0$. We focus on the two eigenvectors associated with the relevant directions in the vicinity of the minimum of the effective potential, *i.e.*, we zoom in onto the region near the minima for plots similar to Fig. 16. We do this for both $\delta w(\varphi)$ and $\delta z(\varphi)$ which we rescale with the form in Eq. (52). We display in Fig. 18 $\delta g(x)/(\alpha + w(\varphi))^2$, which provides a better visualization as we argued before, and $\delta\zeta(x)$, with $x = (\varphi - \varphi_{\min})/\delta(\tilde{\epsilon})$, for both $\lambda = -1/\nu$ (even eigenvector) and $\lambda = -D_\phi$ (odd eigenvector). We first observe that the collapse onto the boundary-layer scaling curves is very good for the range of $\tilde{\epsilon}$ from 0.006 ($d = 1.2$) down to the lowest attainable

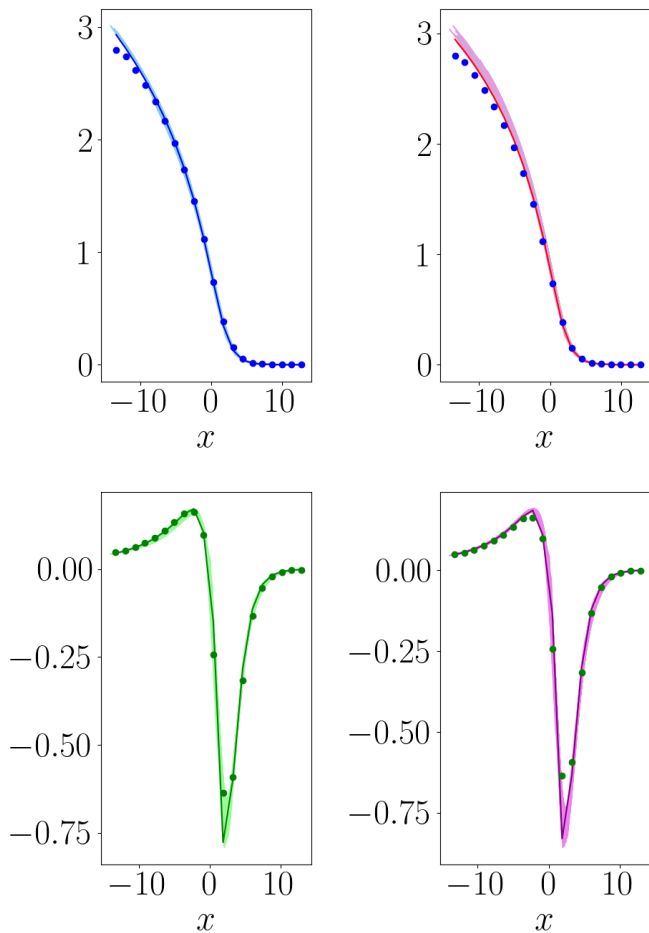


FIG. 18. Zoom in onto the eigenvectors associated with $\lambda = -1/\nu$ (left) and $\lambda = -D_\phi$ (right) in the region near the minimum of the effective potential. The functions $\delta g(x)/g(x)^2 = (1/\delta(\tilde{\epsilon}))\delta w(\varphi)/w(\varphi)^2$ (top panels) and $\delta z(x) = (\delta(\tilde{\epsilon})/\kappa(\tilde{\epsilon}))\delta z(\varphi)$ (bottom panels) are plotted in terms of the boundary-layer variable $x = (\varphi - \varphi_{\min})/\delta(\tilde{\epsilon})$. The full lines are the functions obtained for $d = 1.113$ (which corresponds to $\tilde{\epsilon} = 0.00301$) and the lightly colored lines represent all the eigenvectors between $d = 1.2$ ($\tilde{\epsilon} = 0.006$) and $d = 1.113$ collapsed with the boundary-layer ansatz in Eq. (52). We also plot the first derivatives of the fixed-point functions, $w'(\varphi)/w(\varphi)^2$ divided by $\delta(\tilde{\epsilon})$ (symbols in the top panels) and $z'(\varphi)$ divided by $\kappa(\tilde{\epsilon})/\delta(\tilde{\epsilon})$ (symbols in the bottom panels). The superimposition with the eigenvectors is done with an arbitrary proportionality constant which is different for the two eigenvalues but which is the same for the δw and the δz directions. In these plots we have used the Exponential regulator with a prefactor $\alpha = 1$.

value 0.003 ($d \approx 1.113$). This strongly supports that this boundary-layer scaling persists down to $\tilde{\epsilon} = 0$.

Strikingly, we also find that the eigenvectors for $-1/\nu$ and $-D_\phi$ are virtually superimposable up to a constant proportionality factor which is the same for the perturbation in the w direction and in the z direction. Furthermore, the eigenvectors are extremely close to the deriva-

tive of the associated fixed-point function. As the convergence of the eigenvectors to their form when $\tilde{\epsilon} \rightarrow 0$ appears fast, much faster than the convergence of, say, $1/\nu$ (see Fig. 17), this then gives solid evidence that the asymptotic form of the eigenvectors for both $-1/\nu$ and $-D_\phi$ in the boundary layer are proportional to the derivative of the fixed-point functions. As discussed in Sec. VI C, this implies that the eigenvalues are zero when $\tilde{\epsilon} \rightarrow 0$.

This is exactly what is found in the LPA' approximation and it corroborates that the LPA' scenario is also valid at the ∂^2 level, then supporting that $1/\nu = 0$ in $\tilde{\epsilon} = 0$.

VII. CONCLUSION

In this paper we have pursued our investigation of how the generic nonperturbative approximation of the functional RG that takes the form of a truncated expansion of the running effective-action functional in derivatives of the field around a uniform background is able to describe physical situations in which the long-distance properties are controlled by strongly nonuniform renormalized configurations such as instantons and droplets.

We have focused on the approach to the lower critical dimension d_{lc} in the Z_2 -symmetric scalar φ^4 theory (Ising universality class) and pushed our previous related investigation¹⁴ to the second order of the derivative expansion. The numerical and the analytical analyses require solving two coupled differential equations for the functions of the field characterizing the critical fixed point and both turn out to be much more involved than at the lower order. We are therefore unable to obtain a full control of the numerics (although we can solve the fixed point equations down to relative distance of 10^{-3} of d_{lc}) and of the analytical treatment (although we build on the singular perturbation approach previously developed¹⁴). We nonetheless provide strong evidence that, as at the lower order, the convergence of the fixed-point functions in the limit where $d \rightarrow d_{lc}$ is nonuniform in the field and involves the emergence of a boundary layer of shrinking width near the minima of the effective potential.

As already stressed in the Introduction, nothing guarantees that the approximate NPF RG treatment recovers the exact result $d_{lc} = 1$. The value of d_{lc} is indeed found to depend on the specific form of the IR regulator used to progressively introduce the fluctuations of the field, and for the 3 different forms that we have considered we obtain an optimal value around $0.8 - 0.9$, *i.e.*, below the exact result. This explains why NPF RG analyses directly studying $d = 1$ are unable to describe the expected features of the lower critical dimension of Ising-like models, in contrast to similar studies of the $O(N)$ model where the lower critical dimension of 2 and the Goldstone modes are easily retrieved.^{3,4} A prospect of future NPF RG studies would be to investigate whether one can find a specific

IR regulator that predicts $d_{lc} = 1$ at the second-order of the derivative expansion, which would for instance allow one to study all regimes of quantum barrier tunneling or of the Schmidt transition in a resistively shunted Josephson junction.

Interestingly, the nonuniform convergence and the boundary layer found in the NPF RG treatment provide a mechanism for generating two different small parameters that are nonperturbatively related as $d \rightarrow d_{lc}$: one, denoted here by $\tilde{\epsilon}$, which controls the dimension of the field D_ϕ as it goes to zero and another, $1/\ln(1/\tilde{\epsilon})$, which controls the vanishing of the critical temperature T_c and, plausibly but not fully established, of the inverse correlation length $1/\nu$. This is precisely what is obtained in the RG theory of Bruce and Wallace which directly focuses on the droplet configurations that dominate the critical behavior in low dimensions: $\tilde{\epsilon}$ can be put in correspondence with the critical droplet concentration and $1/\ln(1/\tilde{\epsilon})$ with the fractal dimension of the droplet surface, although no explicit description in terms of droplets is introduced in the truncated derivative expansion of the NPF RG. In any case this confirms the ability of the (approximate) NPF RG to capture, at least partially, the influence of strongly nonuniform field configurations and opens the possibility to study other (more interesting) problems where such configurations are important, such as in systems with quenched disorder.

ACKNOWLEDGMENTS

We thank Adam Rançon for numerous discussions related to this topic over the past years. We acknowledge the support of the Croatian Scientific Foundation grant HRZZ-IP-2022-9423, ‘‘Cogito’’- Partnership Hubert Curien bilateral project with France (LNF and IB) as well as the QuantiXLie Centre of Excellence (LNF and IB), a project cofinanced by the Croatian Government and European Union through the European Regional Development Fund - the Competitiveness and Cohesion Operational Programme (Grant KK.01.1.1.01.0004).

Appendix A: NPF RG flow equations at ∂^2 order

The beta function describing the NPF RG flow of the dimensionless effective potential $u_k(\varphi)$ at ∂^2 order is given by³

$$\beta_u^{(d)}(\varphi; \eta) = 2v_d \ell_0^{(d)}(u''(\varphi); z(\varphi); \eta), \quad (\text{A1})$$

where $v_d^{-1} = 2^{d+1} \pi^{d/2} \Gamma(d/2)$; $\ell_n^{(d)}$ is a (strictly positive) dimensionless threshold function defined by

$$\ell_n^{(d)}(w; z; \eta) = - \left(\frac{n + \delta_{n,0}}{2} \right) \int_0^\infty dy y^{\frac{d}{2}} \frac{\eta r(y) + 2yr'(y)}{(y[z + r(y)] + w)^{n+1}} \quad (\text{A2})$$

where the dimensionless infrared cutoff function (or IR regulator) $r(y)$ is obtained from the dimensionful one, $R_k(q^2)$, which is introduced in Eq. (2), through

$$R_k(q^2) = Z_k k^2 y r(y) \quad \text{with } y = \frac{q^2}{k^2} \quad (\text{A3})$$

with k the running IR cutoff and Z_k the dimensionful field renormalization (from which the running anomalous dimension is defined by $\eta_k = -k \partial_k \ln Z_k$).

From the exact FRG equation for the 2-point 1-PI correlation function evaluated for a uniform field configuration one can extract the beta functional for the dimensionless field renormalization function $z_k(\varphi)$, which when truncated at ∂^2 order reads³

$$\begin{aligned} \beta_z^{(d)}(\varphi; \eta) = & -\frac{4v_d}{d} u''''(\varphi)^2 m_{4,0}^{(d)}(u''(\varphi); z(\varphi); \eta) - \\ & \frac{8v_d}{d} u''''(\varphi) z'(\varphi) m_{4,0}^{(d+2)}(u''(\varphi); z(\varphi); \eta) \\ & - \frac{4v_d}{d} z'(\varphi)^2 m_{4,0}^{(d+4)}(u''(\varphi); z(\varphi); \eta) - 2v_d z''(\varphi) \times \\ & \ell_1^{(d)}(u''(\varphi); z(\varphi); \eta) + 4v_d u''''(\varphi) z'(\varphi) \ell_2^{(d)}(u''(\varphi); z(\varphi); \eta) \\ & + 2v_d \frac{1 + 2d}{d} z'(\varphi)^2 \ell_2^{(d+2)}(u''(\varphi); z(\varphi); \eta), \end{aligned} \quad (\text{A4})$$

where $m_{n,0}^{(d)}$ is another (strictly positive) threshold function defined as

$$\begin{aligned} m_{n,0}^{(d)}(w; z; \eta) = & \frac{1}{2} \int_0^\infty dy y^{\frac{d}{2}} \frac{z + (yr(y))'}{(y[z + r(y)] + w)^n} \left[2\eta(yr(y))' \right. \\ & \left. + 4(y^2 r'(y))' - n \frac{y[z + (yr(y))'] [\eta r(y) + 2yr'(y)]}{y[z + r(y)] + w} \right]. \end{aligned} \quad (\text{A5})$$

To derive Eq. (D4) we have neglected the higher-order terms in Eq. (6) which involve four spatial derivatives and more. The present ∂^2 approximation is fully characterized by the two functions $U_k(\phi)$ and $Z_k(\phi)$, or their dimensionless counterparts, $u_k(\phi)$ and $z_k(\phi)$. (Three more functions are required at the order $O(\partial^4)$, etc.)

Appendix B: Alternative scalings for the field renormalization function in the boundary layer

We briefly discuss alternatives for the scaling of the field renormalization function $z(\varphi)$ in the boundary layer, in which it scales differently than $\kappa(\tilde{\epsilon})/\delta(\tilde{\epsilon})$ with $\kappa(\tilde{\epsilon}) \rightarrow 0$ when $\tilde{\epsilon} \rightarrow 0+$.

1. $z = O(1)$ in the boundary layer

If $z(\varphi) \equiv z(x) = O(1)$ in the boundary layer, then the corresponding fixed-point equation becomes at leading order

$$0 = (2-d)z(x) + d \frac{g'(0)}{g(0)^3} z'(x) - d \left[\frac{z''(x)}{g(x)^2} + 4 \frac{z'(x)}{g(x)} \times \partial_x \left(\frac{1}{g(x)} \right) + \left(2z(x) - \alpha^*(d) \frac{3d-2}{2d} \right) \left(\partial_x \left(\frac{1}{g(x)} \right) \right)^2 \right], \quad (\text{B1})$$

where $\alpha^*(d)$ is a regulator dependent function of d , *e.g.*, for the Theta or Litim regulator $\alpha^* = \alpha$ and for the Exponential regulator $\alpha^* = 2^{-(1+\frac{d}{2})}\alpha$.

In this case one easily shows that, when $x \rightarrow -\infty$, $z(x)$ asymptotically goes as

$$z(x) = z_0 + O\left(\frac{1}{\ln(|x|)}\right), \quad (\text{B2})$$

with

$$z_0 = \alpha^*(d) \frac{3d_l - 2}{4d_l}. \quad (\text{B3})$$

We next have to consider the matching with the solution of the fixed-point equations for φ of $O(1)$ (then dropping the terms in $\tilde{\epsilon}\varphi\partial_\varphi$ and neglecting terms of order $\tilde{\epsilon}$). We solve the latter numerically for φ between 0 and a maximum field φ_M by using the Runge-Kutta method implemented in Wolfram Mathematica. For matching with the boundary-layer solution when $\varphi \gg 1$ yet $x \rightarrow -\infty$, we take the boundary conditions in a field $\varphi_M \gg 1$ satisfying $\varphi_{\min} - \varphi_M \sim (\tilde{\epsilon}\varphi_{\min})^a$ with $0 < a < 1$ and $\varphi_{\min} \sim \sqrt{\ln(1/\tilde{\epsilon})}$ (see Secs. IV and V). Then we choose $w(\varphi_M) \sim \tilde{\epsilon}^{-a} [\ln(1/\tilde{\epsilon})]^{-(1+a)/2} \gg 1$ [see Eqs. (36) and (22)] and $z(\varphi_M) = z_0$ where z_0 is given by Eq. (B3).

We find a unique, stable, solution such that $w(\varphi) \rightarrow 0$ and $z(\varphi) \rightarrow 0$ as $\varphi \rightarrow 0$, which clearly cannot correspond to a physical fixed-point solution at criticality.

2. $z \propto \frac{1}{\delta(\tilde{\epsilon})}$ in the boundary layer

If $z(\varphi) \approx \zeta(x)/\delta(\tilde{\epsilon})$ in the boundary layer, *i.e.*, $\kappa(\tilde{\epsilon}) = O(1)$, the fixed-point equations drastically change because the propagator in the boundary layer now takes the form

$$p(y; w(\varphi), z(\varphi)) \approx \frac{\delta(\tilde{\epsilon})}{g(x) + y[r(y) + \zeta(x)]}, \quad (\text{B4})$$

with ζ and g strictly positive functions of $O(1)$. An important consequence is that the equation for $g(x)$ no longer decouples from that of $\zeta(x)$. Furthermore, the integration over the internal momentum cannot be performed in closed form and the equations remain dependent on the IR regulator.

We do not wish to go into the detail of the corresponding calculations and we just give the main results.

We find that for φ_M in the matching region where $w \gg 1$ and $x \rightarrow -\infty$, w and z should behave as

$$w(\varphi_M) \sim (\varphi_{\min} - \varphi_M)^{-\tau_w} \quad (\text{B5})$$

$$z(\varphi_M) \sim (\varphi_{\min} - \varphi_M)^{-\tau_z}, \quad (\text{B6})$$

and the boundary-layer equations are then dominated by the nontrivial part of the beta functions only if

$$\tau_z > \frac{4 - (4-d)\tau_w}{d}, \quad (\text{B7})$$

in which case the dimensional parts are subleading. This requirement seems more natural than having the fixed-point equations dominated by their trivial dimensional part.

We then solved numerically for φ between 0 and φ_M the equations derived for fields of $O(1)$ by neglecting terms in $\tilde{\epsilon}\varphi\partial_\varphi$. With boundary conditions in φ_M of the form given by Eqs. (B5, B6, B7) and with a range of regulator prefactors $\alpha = O(1)$, no physical fixed-point solution was found, whatever the choice of τ_w, τ_z . Indeed, $z(\varphi \rightarrow 0)$ always becomes very large, in contradiction with the condition that $z(\varphi = 0) = 1$.

Appendix C: Boundary-layer periodic solutions

We note that the equations derived for fields of $O(1)$ when dropping the terms in $\tilde{\epsilon}\varphi\partial_\varphi$, *i.e.*, formally setting $\tilde{\epsilon} = 0$ in the equations, also admit boundary-layer solutions around the minimum φ_* of the periodic solution $\bar{w}(\varphi)$. We call them “boundary-layer periodic” solutions. Besides the fact that they may be interesting when considering the matching procedure between the periodic solution $(\bar{w}(\varphi), \bar{z}(\varphi))$ of the $\tilde{\epsilon} = 0$ equations and the (physical) boundary-layer fixed-point equations, they may also be relevant in the context of the Sine Gordon model.¹³²⁷

Denoting the width of the “periodic boundary” layer by $\bar{\delta}$ and assuming that

$$\begin{aligned} \bar{w}(\varphi) &= \frac{\bar{g}(\bar{x})}{\bar{\delta}} \\ \bar{z}(\varphi) &= \frac{\bar{\kappa} \bar{\zeta}(\bar{x})}{\bar{\delta}} \end{aligned} \quad (\text{C1})$$

with $\bar{x} = (\varphi - \varphi_*)/\bar{\delta}$, we can repeat the derivation of the boundary-layer fixed point equations but starting from

the equations with $\tilde{\epsilon} = 0$. This gives at leading order

$$\begin{aligned} 0 &= -\bar{g}(\bar{x}) + \partial_{\bar{x}}^2 \left(\frac{1}{\bar{g}(\bar{x})} \right) \\ 0 &= \frac{(2-d)\bar{\zeta}(\bar{x})}{d} - \left[\frac{\bar{\zeta}''(\bar{x})}{\bar{g}(\bar{x})^2} + 4 \frac{\bar{\zeta}'(\bar{x})}{\bar{g}(\bar{x})} \partial_{\bar{x}} \left(\frac{1}{\bar{g}(\bar{x})} \right) \right. \\ &\quad \left. + 2\bar{\zeta}(\bar{x}) \left(\partial_{\bar{x}} \left(\frac{1}{\bar{g}(\bar{x})} \right) \right)^2 \right]. \end{aligned} \quad (\text{C2})$$

The only difference with the physical boundary-layer equations is the absence of the term in $\zeta'(x)$ in the second equation: compare with Eq. (25).

Similarly to what is done in Sec. IV, we proceed to a change of variable,

$$\bar{X}(\bar{x}) = \partial_{\bar{x}} \left(\frac{1}{\bar{g}(\bar{x})} \right), \quad (\text{C3})$$

and we introduce the functions

$$\bar{a}(\bar{X}) \equiv \frac{1}{\bar{g}(\bar{x})} \quad (\text{C4})$$

$$\bar{b}(\bar{X}) \equiv \frac{\bar{\zeta}(\bar{x})}{\bar{g}(\bar{x})^2}, \quad (\text{C5})$$

so that the periodic boundary-layer equations read

$$\bar{a}'(\bar{X}) - \bar{X} \bar{a}(\bar{X}) = 0 \quad (\text{C6})$$

$$\bar{b}''(\bar{X}) - \bar{X} \bar{b}'(\bar{X}) - \frac{2+d}{d} \bar{b}(\bar{X}) = 0. \quad (\text{C7})$$

Because they correspond to the periodic solution, the solution of the above equations should be symmetric in the inversion $\bar{X} \rightarrow -\bar{X}$ and we find them as

$$\bar{a}(\bar{X}) = \bar{a}_0 e^{\frac{\bar{X}^2}{2}} \quad (\text{C8})$$

$$\bar{b}(\bar{X}) = {}_1F_1\left(\frac{q}{2}, \frac{1}{2}, \frac{\bar{X}^2}{2}\right) \tilde{b}, \quad (\text{C9})$$

with \bar{a}_0 and \tilde{b} some constants and $q = (2+d)/d$ as for the physical boundary-layer solution.

We can now study the matching of the periodic and physical boundary-layer solutions in the matching region where $\bar{x} \rightarrow -\infty$ (for the former) and $x \rightarrow -\infty$ (for the latter). Then, \bar{X}, X go to $-\infty$ as $-\sqrt{2 \ln(|\bar{x}|)}$ and $-\sqrt{2 \ln(|x|)}$ respectively. The leading orders correspond provided one chooses $\bar{a}_0 = \sqrt{2\pi}$ and $\tilde{b} = \hat{b} \lim_{X \rightarrow -\infty} \frac{H_{-q}(\frac{X}{\sqrt{2}})}{{}_1F_1(\frac{q}{2}, \frac{1}{2}, \frac{X^2}{2})}$, where we recall that $\hat{b} = 2^{q-1} \sqrt{\pi} \Gamma((1+q)/2)$ (see Sec. IV); this applies for any value of q .

Appendix D: System of eigenvalue equations at ∂^2 order

To obtain the eigenvalue equations we start from the dimensionless flow equations of $w_k(\varphi)$ and $z_k(\varphi)$,

$$\begin{aligned} \partial_t w_k(\varphi)|_{\varphi} &= -(2 - \eta_k) w_k(\varphi) + \frac{(d-2 + \eta_k)}{2} \varphi w'_k(\varphi) \\ &\quad + \beta_w^{(d)}(\varphi; \eta_k) \end{aligned} \quad (\text{D1})$$

and

$$\partial_t z_k(\varphi)|_{\varphi} = \eta_k z_k(\varphi) + \frac{(d-2 + \eta_k)}{2} \varphi z'_k(\varphi) + \beta_z^{(d)}(\varphi; \eta_k), \quad (\text{D2})$$

where from Appendix A,

$$\begin{aligned} \beta_w^{(d)}(\varphi; \eta) &\equiv \beta_w^{(d)}(w(\varphi), w'(\varphi), w''(\varphi); z(\varphi), z'(\varphi), z''(\varphi); \eta) \\ &= 2v_d \partial_{\varphi}^2 \ell_0^{(d)}(w(\varphi); z(\varphi); \eta) \end{aligned} \quad (\text{D3})$$

and

$$\begin{aligned} \beta_z^{(d)}(\varphi; \eta) &\equiv \beta_z^{(d)}(w(\varphi), w'(\varphi); z(\varphi), z'(\varphi), z''(\varphi); \eta) \\ &= -\frac{4v_d}{d} w'(\varphi)^2 m_{4,0}^{(d)}(w(\varphi); z(\varphi); \eta) - \\ &\quad \frac{8v_d}{d} w'(\varphi) z'(\varphi) m_{4,0}^{(d+2)}(w(\varphi); z(\varphi); \eta) \\ &\quad - \frac{4v_d}{d} z'(\varphi)^2 m_{4,0}^{(d+4)}(w(\varphi); z(\varphi); \eta) - 2v_d z''(\varphi) \times \\ &\quad \ell_1^{(d)}(w(\varphi); z(\varphi); \eta) + 4v_d u'''(\varphi) z'(\varphi) \ell_2^{(d)}(w(\varphi); z(\varphi); \eta) \\ &\quad + 2v_d \frac{1+2d}{d} z'(\varphi)^2 \ell_2^{(d+2)}(w(\varphi); z(\varphi); \eta). \end{aligned} \quad (\text{D4})$$

The above beta functions can be more explicitly obtained by taking derivatives with respect to w and z of Eqs. (A2) and (A5). Note that $\beta_z^{(d)}$ does not depend on w'' .

After inserting $w_k(\varphi) = w(\varphi) + k^\lambda \delta w(\varphi)$, $z_k(\varphi) = z(\varphi) + k^\lambda \delta z(\varphi)$, $\eta_k = \eta + k^\lambda \delta \eta$, where w , z , and η are the fixed-point quantities, and linearizing the FRG flow equations, we obtain Eq. (47) with

$$\begin{aligned} A_1(\varphi) &= w(\varphi) + \frac{1}{2} \varphi w'(\varphi) + \partial_{\eta} \beta_w^{(d)}(\varphi; \eta), \\ A_2(\varphi) &= z(\varphi) + \frac{1}{2} \varphi z'(\varphi) + \partial_{\eta} \beta_z^{(d)}(\varphi; \eta), \end{aligned} \quad (\text{D5})$$

as well as

$$\begin{aligned} a_{11}(\varphi) &= \partial_w \beta_w^{(d)}(w, w', w''; z, z', z'' \eta), \\ a_{12}(\varphi) &= \partial_z \beta_w^{(d)}(w, w', w''; z, z', z'' \eta), \\ a_{21}(\varphi) &= \partial_w \beta_z^{(d)}(w, w'; z, z', z'' \eta), \\ a_{22}(\varphi) &= \partial_z \beta_z^{(d)}(w, w'; z, z', z'' \eta), \end{aligned} \quad (\text{D6})$$

where $w, w', w'', z, z',$ and z'' are formally considered as independent variables.

Similarly,

$$\begin{aligned}
b_{11}(\varphi) &= \partial_{w'} \beta_w^{(d)}(w, w', w''; z, z', z''\eta), \\
b_{12}(\varphi) &= \partial_{z'} \beta_w^{(d)}(w, w', w''; z, z', z''\eta), \\
b_{21}(\varphi) &= \partial_{w'} \beta_z^{(d)}(w, w'; z, z', z''\eta), \\
b_{22}(\varphi) &= \partial_{z'} \beta_z^{(d)}(w, w'; z, z', z''\eta),
\end{aligned} \tag{D7}$$

and

$$\begin{aligned}
c_{11}(\varphi) &= \partial_{w''} \beta_w^{(d)}(w, w', w''; z, z', z''\eta), \\
c_{12}(\varphi) &= \partial_{z''} \beta_w^{(d)}(w, w', w''; z, z', z''\eta), \\
c_{21}(\varphi) &= \partial_{w''} \beta_z^{(d)}(w, w'; z, z', z''\eta), \\
c_{22}(\varphi) &= \partial_{z''} \beta_z^{(d)}(w, w'; z, z', z''\eta).
\end{aligned} \tag{D8}$$

More explicitly, the c_{ij} 's are given by

$$\begin{aligned}
c_{11}(\varphi) &= -2v_d \ell_1^{(d)}(w(\varphi); z(\varphi); \eta), \\
c_{12}(\varphi) &= 2v_d \partial_z \ell_0^{(d)}(w; z; \eta)|_{w=w(\varphi), z=z(\varphi)}, \\
c_{21}(\varphi) &= 0, \\
c_{22}(\varphi) &= -2v_d \ell_1^{(d)}(w(\varphi); z(\varphi); \eta),
\end{aligned} \tag{D9}$$

so that one checks that the matrix is invertible with determinant $[2v_d \ell_1^{(d)}(w(\varphi); z(\varphi); \eta)]^2 > 0$. The explicit expressions of the other functions are also trivially derived but are not worth displaying.

From the above equations, one can see that by construction, the A_i 's, a_{ij} 's and c_{ij} 's are even in φ while the b_{ij} 's are odd.

Appendix E: Two zero eigenmodes in the LPA' approximation when $\tilde{\epsilon} \rightarrow 0$

We revisit here the leading eigenvalues around the fixed point in the LPA' approximation when $\tilde{\epsilon} \rightarrow 0$. The equations to be considered are the flow equation for the square-mass function $w_k(\varphi)$ and for the running anomalous dimension η_k which is defined by a prescription at the running minimum $\varphi_{\min, k}$ of the potential,¹⁴

$$\eta_k = \frac{4v_d}{d} w'(\varphi_{\min, k})^2 m_{4,0}^{(d)}(w(\varphi_{\min, k}); \eta_k) \tag{E1}$$

where $m_{4,0}^{(d)}(w; \eta)$ is given by Eq. (A5) with $n = 4$ and $z = 1$. We study the perturbation around the fixed point $w_k(\varphi) = w(\varphi) + k^\lambda \delta w(\varphi)$ and $\eta_k = \eta + k^\lambda \delta \eta$, and we do

so through a singular perturbation treatment: see also [14].

In the boundary layer there is a solution at leading order when $\tilde{\epsilon} \rightarrow 0$ with eigenvalue $\lambda = 0$ and $\delta w(\varphi) \propto w'(\varphi)$. One can easily check that this corresponds also to $\delta \eta = 0$.

The issue to be resolved is how can one extend this eigenmode to the whole range of variation of φ . We therefore consider the eigenvalue equation for $\delta w(\varphi)$ associated with $\lambda = 0$ and $\delta \eta = 0$ in the region where $\varphi = O(1)$ when setting then formally $\tilde{\epsilon} = 0$. The equation is then

$$0 = \delta w(\varphi) - \frac{2v_d}{d} \partial_\varphi^2 [-\ell_1^{(d)}(\bar{w}(\varphi)) \delta w(\varphi)]. \tag{E2}$$

where we have used that $\eta = 2 - d + O(\tilde{\epsilon})$ and that $\partial_w \ell_0^{(d)}(w) = -\ell_1^{(d)}(w)$. The corresponding equation for the fixed-point function is the same as Eq. (38) with $z = 1$, and it has a periodic solution $\bar{w}(\varphi)$ with half-period φ_* which becomes asymptotically close to φ_{\min} and diverges as $\sqrt{\ln(1/\tilde{\epsilon})}$ when $\tilde{\epsilon} \rightarrow 0$.

We look for a solution of Eq. (E2) of the form $\delta w(\varphi) = c(\varphi) \bar{w}'(\varphi)$. We then arrive at the equation

$$0 = 2\partial_\varphi^2 \ell_0^{(d)}(\bar{w}(\varphi)) c'(\varphi) + \partial_\varphi \ell_0^{(d)}(\bar{w}(\varphi)) c''(\varphi), \tag{E3}$$

whose generic solution is

$$c'(\varphi) = \frac{A}{[\partial_\varphi \ell_0^{(d)}(\bar{w}(\varphi))]^2}, \tag{E4}$$

with A some constant. We immediately see that $A = 0$ corresponding to $c(\varphi) = K$ is solution and corresponds to an odd eigenvector $\delta w(\varphi)$ under the inversion of φ . This eigenvector can be matched with the solution in the boundary layer and it is associated with the eigenvalue $\lambda = -(d-2+\eta)/2 \propto \tilde{\epsilon} \rightarrow 0$: see Sec. VI A.

When $A \neq 0$, $c'(\varphi)$ is an even function that diverges as $1/\varphi^2$ when $\varphi \rightarrow 0$. Furthermore it varies slowly and is vanishingly small in the whole region $1 \ll \varphi \ll \varphi_*$. One can therefore choose a primitive $c(\varphi)$ which is odd and behaves as $1/\varphi$ when $\varphi \rightarrow 0$,

$$c(\varphi) \propto -\frac{1}{\varphi} + \int_0^\varphi d\varphi' \left(\left[\frac{\ell_1^{(d)}(\bar{w}_0) \bar{w}_0''}{\ell_1^{(d)}(\bar{w}(\varphi')) \bar{w}'(\varphi')} \right]^2 - \frac{1}{\varphi'^2} \right) \tag{E5}$$

where the integral is convergent when $\varphi \rightarrow 0$ as $\bar{w}'(\varphi') = \bar{w}_0'' \varphi + O(\varphi^2)$. This leads to the behavior described in Eq. (58). The resulting eigenfunction $f(\varphi) = c(\varphi) \bar{w}'(\varphi)$ is even and is well defined in $\varphi = 0$ (the $1/\varphi$ of $c(\varphi)$ is then compensated by $w'(\varphi) \propto \varphi$).

^a balog@ifs.hr

^b Inf@phy.hr

- ^c maroje.marohnic@gmail.com
^d tarjus@lptmc.jussieu.fr
- ¹ A. D. Bruce and D. J. Wallace, *Phys. Rev. Lett.* **47**, 1743 (1981).
 - ² A. D. Bruce and D. J. Wallace, *Journal of Physics A: Mathematical and General* **16**, 1721 (1983).
 - ³ J. Berges, N. Tetradis, and C. Wetterich, *Phys. Rep.* **363**, 223 (2002).
 - ⁴ N. Dupuis, L. Canet, A. Eichhorn, W. Metzner, J. Pawłowski, M. Tissier, and N. Wschebor, *Phys. Rep.* **910**, 1 (2021).
 - ⁵ R. Peierls, *Mathematical Proceedings of the Cambridge Philosophical Society* **32**, 477–481 (1936).
 - ⁶ K.-I. Aoki, A. Horikoshi, M. Taniguchi, and H. Terao, *Progress of Theoretical Physics* **108**, 571 (2002).
 - ⁷ A. Kapoyannis and N. Tetradis, *Physics Letters A* **276**, 225 (2000).
 - ⁸ M. Weyrauch, *Journal of Physics A: Mathematical and General* **39**, 649 (2005).
 - ⁹ D. Zappalá, *Physics Letters A* **290**, 35 (2001).
 - ¹⁰ A. Bonanno, A. Codello, and D. Zappalá, *Annals of Physics* **445**, 169090 (2022).
 - ¹¹ C. Rulquin, P. Urbani, G. Biroli, G. Tarjus, and M. Tarzia, *Journal of Statistical Mechanics: Theory and Experiment* **2016**, 023209 (2016).
 - ¹² I. Nándori, I. G. Márián, and V. Bacsó, *Phys. Rev. D* **89**, 047701 (2014).
 - ¹³ R. Daviet and N. Dupuis, *Phys. Rev. B* **108**, 184514 (2023).
 - ¹⁴ L. N. Farkaš, G. Tarjus, and I. Balog, *Phys. Rev. E* **108**, 054107 (2023).
 - ¹⁵ H. Ballhausen, J. Berges, and C. Wetterich, *Physics Letters B* **582**, 144 (2004).
 - ¹⁶ K. G. Wilson and J. B. Kogut, *Phys. Rept.* **12**, 75 (1974).
 - ¹⁷ D. F. Litim, *Phys. Rev. D* **64**, 105007 (2001).
 - ¹⁸ I. Balog, H. Chaté, B. Delamotte, M. Marohnić, and N. Wschebor, *Phys. Rev. Lett.* **123**, 240604 (2019).
 - ¹⁹ L. Canet, B. Delamotte, D. Mouhanna, and J. Vidal, *Phys. Rev. B* **68**, 064421 (2003).
 - ²⁰ C. Wetterich, *Phys. Lett. B* **301**, 90 (1993).
 - ²¹ C. Wetterich, *Zeitschrift für Physik C* **60**, 461 (1993).
 - ²² C. Wetterich, *Zeitschrift für Physik C Particles and Fields* **57**, 451 (1993).
 - ²³ J.-P. Blaizot, R. Méndez-Galain, and N. Wschebor, *Phys. Lett. B* **632** (2006), <https://doi.org/10.1016/j.physletb.2005.10.086>.
 - ²⁴ J. Kevorkian and J. D. Cole, *Perturbation Methods in Applied Mathematics*, Applied Mathematical Sciences, Vol. 34 (Springer-Verlag, New York, 1981).
 - ²⁵ J. K. Hunter, *Asymptotic Analysis and Singular Perturbation Theory*, Technical Report (University of California, Davis, Department of Mathematics, Davis, CA, 2004) available at <http://www.math.ucdavis.edu/~hunter/notes/asy.pdf>.
 - ²⁶ T. R. Morris, *Physics Letters B* **334**, 355 (1994).
 - ²⁷ Private communication with Romain Daviet.